CFD Based Comparison of Flutter Effect in Supersonic Wing Designs at Steady Aerodynamic Condition

Varunkumar K S[1] , Nikhil N Gangamkote[2]
[1]Dept of Mechanical Engineering
[2]Dept of Aerospace Engineering
[1]Madras Institute of Technology, Anna University
[2]M S Ramaiah University of Applied Sciences

Abstract- *This research paper presents a numerical methodology and analysis to study the aeroelastic effect of flutter, which is a self-exciting oscillation that can occur on wings at high speeds; particularly referred to as the twist along its axis of stiffness. The focus of this study is to understand the interaction between aerodynamic forces and the structural flexibility of the wing, which can lead to the flutter effect, extensively visible in unsteady aerodynamics. After conducting a detailed study, it is clear that the flutter, an unstable aeroelastic phenomenon, can occur even under steady aerodynamic conditions similar to the conventional results shown by unsteady aerodynamics. This phenomenon is possible if the wing is designed to correspond with the thin airfoil theory, which involves a minimal thickness of the wing. To investigate this phenomenon, two wings of feasible dimensions were designed with standard airfoils, including the DAVIS BASIC B-24 WING Airfoil and a customized diamond wedge airfoil. High-precision Computational fluid dynamic simulations were conducted using ANSYS (FLUID FLOW FLUENT) to analyse the effects of lift and drag for various angles of attack, flowlines, vortices and shock wave propagation. STATIC STRUCTURAL and SYSTEM COUPLING methods were also performed to observe the static deformation of the sheet metal design due to the aerodynamic loading (Fluid-Structure interaction) under supersonic conditions, neglecting the effect of gravity. The findings of this study provide insights into the flutter effect and its impact on wing design at high speeds.*

Keywords- Flutter effect, Aeroelasticity, Steady Aerodynamics, Computational Fluid dynamics, Supersonic speed conditions, Fluid-Structure interaction.

I. INTRODUCTION

For any aircraft structure, aerodynamic loading in correspondence with Elastic deformation induced by various stresses leads to the fluttering of that particular structure. Fluttering usually occurs at the expense of inertial loads (Dynamic conditions). The flutter effect is an Aeroelastic effect that occurs at high-speed manoeuvring, rotations and unavoidable stalls, predominantly on the aircraft wings which are not able to withstand the air penetrations. Because of this, the self-excitation of the wing is vividly seen in the waving movement of the wing. Generally, flutter is caused by the detrimental interaction between elastic structural dynamics and unsteady aerodynamics to be precise. There is no wonder that steady aerodynamics provide these astonishing flutter effects provided the thickness of the aircraft wing is negligible relative to the span of the wing. Flutter occurs when the natural frequency of the structure matches the frequency of the aerodynamic forces acting on it. This causes the structure to vibrate, and the vibration generates more aerodynamic forces that further excite the vibration, leading to an unstable feedback loop that can cause the structure to fail if left unchecked. Steady aerodynamics refers to the study of the behaviour of fluids when the velocity and direction of the flow remain constant over time. This type of flow can be analysed using the principles of statics, where the forces and pressures acting on an object in the flow are in equilibrium. In steady flow, the properties of fluid such as density, viscosity, and pressure are assumed to be constant throughout the flow field, and the flow is typically analysed using simplified mathematical models.

The Navier-Stokes equations provide the basic explanation of energy associated with the flow behaviour. The Unsteady aerodynamic models account for flow hysteresis, including unsteady attached flow, trailing edge flow separation, dynamic stall and flow reattachment.

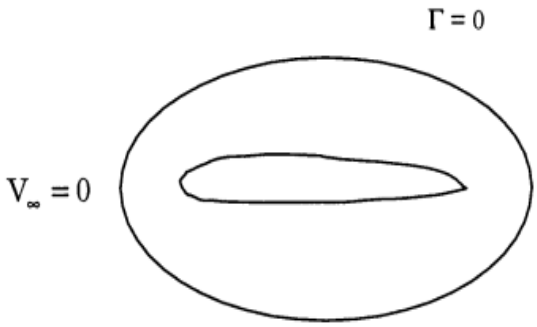

Fig. 1: Representation of fluid at rest relative to the airfoil

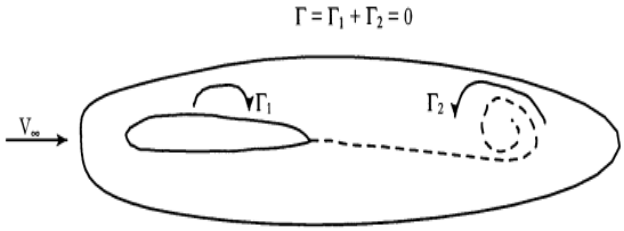

Fig. 2: Representation of forced fluid leading to the formation of vortices at the trailing edge [1]

[**The above images are posted with a copyright mention from the content of the Massachusetts Institute of Technology. Any further reference from the source has been mentioned appropriately**]

The angle of attack is the angle used to describe this orientation. When looking at the two-dimensional flow around an airfoil, as above, aerodynamicists define it is the angle between the main direction of the airflow, *v* and the chord c of the airfoil.

Static aeroelasticity deals with steady fluid–structure interaction problems where coupling effects act in both directions, i.e., the airflow generates distortions of an elastic body in the airstream, and the distortions change the airstream parameters, resulting in the closed loop of loads and deformations.**[7]**

A. Drag analysis under supersonic conditions[8]

At supersonic speeds, aircraft drag is composed of
1. the skin-friction drag,
2. the wave-drag-due-to-thickness (or volume), also known as the zero-lift wave drag, and
3. the drag-due-to-lift

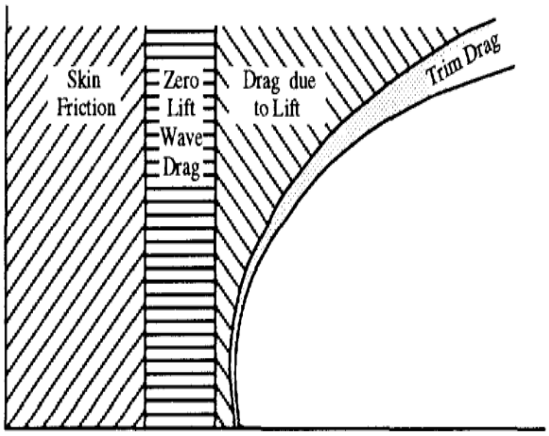

Fig. 3: Representation of types of drag [14]

B. Aircraft Materials

The metals used in the aircraft manufacturing industry include steel, aluminium, titanium and their alloys. Aluminium alloys are characterised by having lower density values compared to steel alloys (around one-third), with good corrosion resistance properties**.** Thus, Aluminium alloy has been incorporated into this design and analysis.

II. GOVERNING EQUATIONS AND THEOREMS

Non-Linear dynamics have been inculcated here since the deformations on the wings are complex because we intend to understand the effects of aerodynamic loading on the sheet metal design to study the excitation/vibration as soon as the wing reaches the resonant frequency of the penetrated air layers. As per ANSYS CFD, Linear models assume that the relationship between inputs and outputs is linear, meaning that the changes in the output are proportional to the corresponding changes in the input, which is not agreeable under this analysis. Even though the fluid flow is considered to be ideal, the vortices created and shockwave propagation necessarily changes the result/output on any further varied input. Thus, we consider Non-Linear dynamics.

A. The Navier-Stokes equation

To understand how fluids move in a computational fluid dynamics (CFD) model, it's essential to grasp flow parameters and behaviours. The Navier-Stokes energy equations serve as the foundation for this understanding, simplifying the analysis of flow behaviour in different fluid systems. When dealing with complex systems, using a numerical approach with these equations is crucial for ensuring accurate simulations. Think of the Navier-Stokes equations as the mathematical tool that helps us make sense of how viscous, incompressible fluids flow. They are derived

from the basic principles of mass, momentum, and energy conservation, which govern how fluids move. These equations aren't just theoretical concepts; they have real-world applications in fields like vehicle design, pipe flow modelling, airfoil design, and more. So, by following the principles of mass, momentum, and energy conservation, the Navier-Stokes equations provide a valuable framework for understanding fluid motion in various practical scenarios.

1. Continuity equation

Within a controlled volume, the mass of the flow remains constant with time. This is the law of conservation of mass and can be expressed as:

$$\frac{\partial \rho}{\partial t} + \nabla \cdot \left(\rho \vec{V}\right) = 0 \quad (1)$$

V is the velocity and ρ is the density.

2. Newton's second law of motion (F=ma) or the momentum equation The change of momentum over time is equal to the sum of forces acting on the system. This Navier-Stokes equation is reflective of the law of conservation of momentum. The momentum equation can be expressed as:

$$\frac{\partial}{\partial t}\left(\rho \vec{V}\right) + \nabla \cdot \left(\rho \vec{V} \otimes \vec{V}\right) = -\nabla p + \nabla \cdot \bar{\bar{\tau}} + \rho \vec{f} \quad (2)$$

τ is the viscous stress and f represents the force per unit mass. Since we are not focussing on the thermal aspect of the wing at supersonic conditions, we might neglect the thermodynamic relation with Navier-Stokes equations.

B. Lift and drag

In ANSYS, the lift and drag forces are typically obtained by integrating the pressure and shear stress distributions over the body surface using numerical methods such as the finite volume method. Using these forces, the lift and drag coefficients are calculated as follows:

- **Lift coefficient calculation**

$$F = \frac{1}{2}\rho v^2 S_{ref} C_L \quad (3)$$

- **Drag Coefficient calculation**

$$D = \frac{1}{2}\rho v^2 S_{ref} C_d \quad (4)$$

Substituting all the known values, C_L and C_d are calculated **[1]**

Since we focus on the calculation of lift and drag forces, the C_L and C_d values' formulations are mentioned here as they might pave the way for newer numerically formulated results on topics of similar interests shortly.

C. Kutta-Joukowski Theorem **[16]**

The Kutta-Joukowski theorem states that the force experienced by a body in a uniform stream is equal to the product of the fluid density, stream velocity, and circulation and has a direction perpendicular to the stream velocity. In order to find the force on a body that is submerged in a streaming fluid (or, equivalently, on a body moving through a stationary fluid), it is necessary to know the value of the circulation. However, the theory indicates that the geometry of the body and the stream velocity does not determine the circulation.

Even though it was initially used for spinning cylinders, these results were extended to airfoils as the curvature of the airfoil and its angle made it possible to rotate the flow around the body.

The lift per unit span of an airfoil is given by:

$$L' = \rho_\infty V_\infty \Gamma \quad (5)$$

D. Thin airfoil theory

Thin airfoil theory is a simple theory of airfoils that relates AOA to lift for incompressible, Inviscid flows.

ASSUMPTION:

1) AOA is small
2) Infinite span of wing and negligible thickness

To correspond with the assumption; Here in this paper, a sheet metal design of wings with a thickness of 1 mm which is relatively very small compared to the span of the wing has been taken into study.

The lift only depends on the mean angle of attack, whereas the drag splits into three components. Namely, a drag due to thickness, a drag due to lift, and a drag due to camber. All these results are formulated by the shock expansion theory.

E. Shock expansion theory [15]

The **shock-expansion theory** general method for computing the pressure variations on a supersonic diamond-wedged airfoil, and is applicable as long as the flow is incompressible to subsonic speeds, and the shock waves remain attached to the airfoil. However, the results of this theory cannot generally be expressed in a concise analytic form. The theory is mostly used to obtain numerical solutions. However, if the airfoil is thin, and the angle of attack is small. In this situation, shock-expansion theory can be considerably simplified by using approximate expressions for weak shocks:

$$\frac{\Delta p}{p} \simeq \left(\frac{\gamma \mathrm{Ma}^2}{\sqrt{\mathrm{Ma}^2-1}}\right) \Delta\Theta 1 \quad (6)$$

It is convenient to define a dimensionless quantity known as the pressure coefficient:

$$C_p = \frac{p-p_1}{q_1} \quad (7)$$

where $q_1 = (1/2)\rho_1 w_1^2$

Given that the upstream sound speed is $c_1 = \sqrt{\gamma p_1/\rho_1}$, and $\mathrm{Ma}_1 = w_1/c_1$, we obtain

$$C_p = \frac{2}{\gamma \mathrm{Ma}_1^2}\frac{p-p_1}{p_1} \quad (8)$$

The above equation can be simplified and expressed in terms of $\Theta 1$ as follows:

$$C_p = \frac{2*\theta 1}{\sqrt{\mathrm{Ma}_1^2-1}} \quad (9)$$

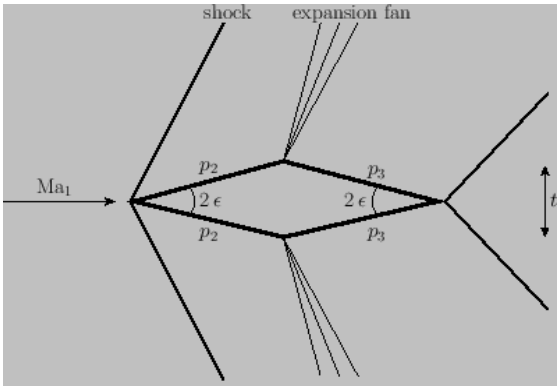

Fig. 4: Geometric representation of diamond wedge airfoil

III. METHODOLOGY

A. Design Approach

This paper reads a comparative study of the flutter effect on 2 wings that were designed 3-dimensionally with presumed dimensions using CATIA V5R21. The design of this wing is of no practical significance as it deals with a sheet metal design providing a thickness of 1 mm for both wings but this may widen out the advancement in research approach towards analyses. Both these wings have been designed using solid modelling and a suitable pocket is made.

In this regard, a symmetric diamond wedge airfoil/wing has been designed with the following considerations:

1) airfoil angle = 20°
2) distance between leading and trailing edge at wing root = 375 mm
3) distance between leading and trailing edge at wing tip = 93.75mm
4) Shortest distance between wing root to tip = 675 mm
5) Swept angle = 18.13°

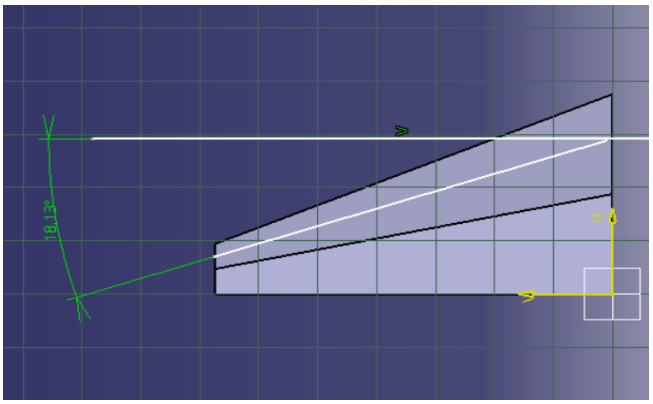

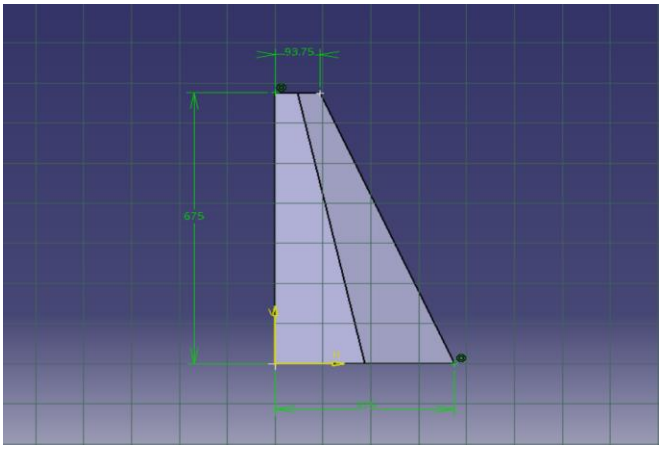

Fig. 5: Dimensional representation of Diamond wedged airfoil

Having named the other wing as WING 2, the dimensions read as follows:

1) distance between leading and trailing edge at wing root = 500mm
2) distance between leading and trailing edge at wing tip = 331mm
3) Shortest distance between wing root to wing tip = 685.5 mm
4) Swept angle = 43.165°

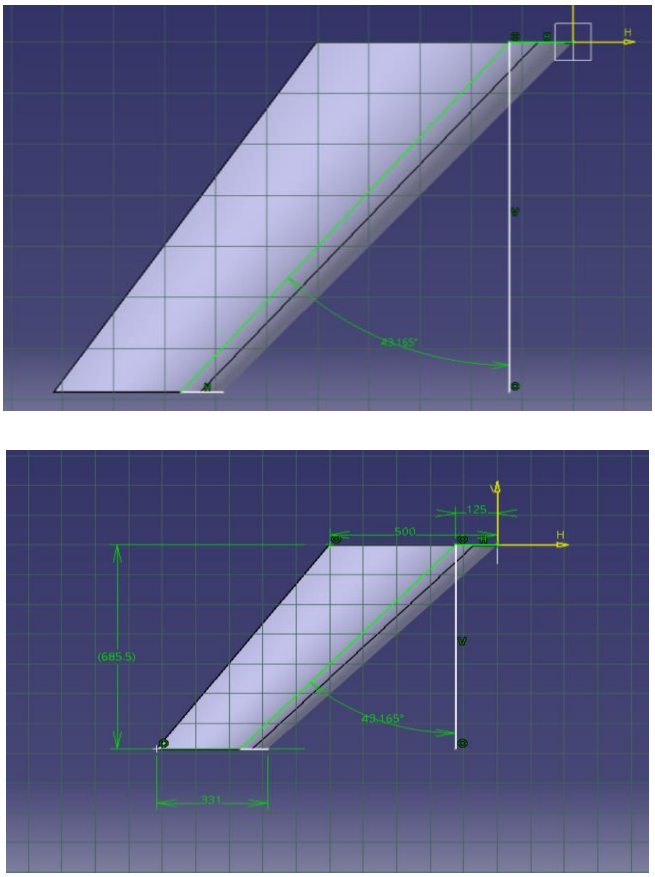

Fig. 6: Dimensional representation of Wing 2

B. CFD Methodology

ANSYS 2022 R1 has been used here to solve the problem upheld,numerically and through simulations to better understand the flow over the wings being designed. Computational fluid dynamics solve both linear and non-linear dynamic cases using partial differential equations provided by the Navier-Stokes theorem. Even though the flow of ideal fluid is laminar and steady but it is no doubt that the production of vortices and propagation of shock waves leads to turbulence in the flow thus bringing non-linear dynamic equations into account.

B.1 Fluid Flow (Fluent) Setup

The Fluid Flow (Fluent) is an Analysis system in ANSYS Workbench, which is a valuable tool for studying the flow of fluid around an object of interest. To initiate the analysis process, the corresponding geometry is imported in .igs format, followed by the creation of an appropriate fluid domain. The shape of the fluid domain plays a crucial role in defining the flow of fluid from the far field towards the target object. A fluid domain is used to define a region of the computational domain occupied by a vacuum or by a fluid specified by its material properties.

Followed by domain creation is Meshing. Mesh generation is the process of producing a two-dimensional and three-dimensional grid, which is then performed. It involves dividing complex geometries into elements that can be used to discretize the domain. Meshing ensures precision in the results, and a good quality finer mesh is the key.

Once the Meshing is done, Boundary conditions as per the analyser's requirement are been fed to the fluent through "Setup".Boundary conditions are then fed to the Fluent through the "Setup" process, which specifies the behaviour of fluid flow at the boundaries of the computational domain. In this research paper, a pressure-based approach was used to focus on the study of aeroelasticity.The fed boundary conditions serve as inputs for the calculation of flow results. Once all the boundary conditions are fed, the calculations are run, and the results are fully converged suitably up to a certain number of iterations. The required contours, plots, and other results are then available for analysis.In summary, the Fluid Flow (Fluent) system in ANSYS Workbench is an effective tool for studying fluid flow, and this paper highlights the crucial steps involved in the process, such as geometry import, fluid domain creation, meshing, boundary condition setup, and calculation of flow results.

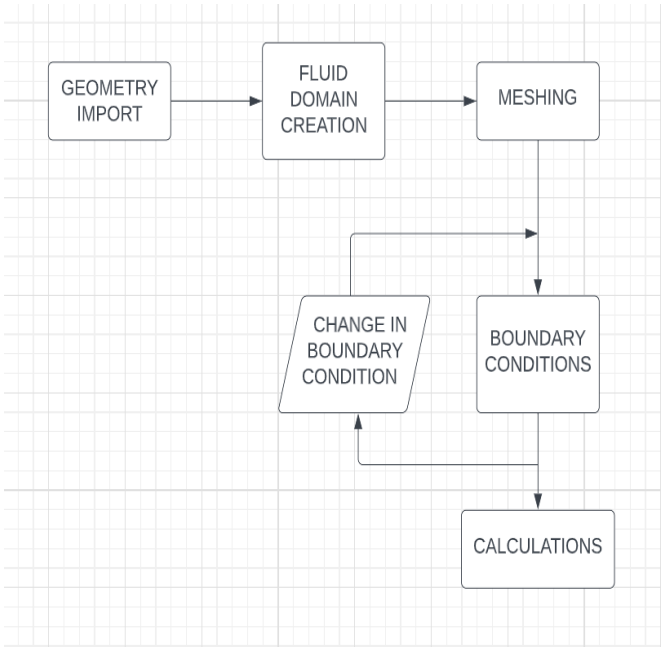

Fig. 7: Schematic representation of the FLUENT approach

B.2 Static Structural Coupling Analysis

ANSYS Static Structural is a finite element analysis tool that is used to analyse and solve static and quasi-static structural problems. This tool is used to analyse the behaviour of solid structures under various load conditions. Material selection from the Engineering data book serves to be the primary step to assign a material to the object of interest.The geometry of the structure is imported as a .igs file into the software as done previously in FLUENT. Even though the mesh is already generated for Fluid flow (FLUENT), another mesh is demanded by Static structural as the software uses the finite element method (FEM) to discretize the structure into small elements so as to provide precise results on deformation, stress, strain and so on. Then, the boundary conditions are applied to the structure as per the requirement. Once the boundary conditions are defined in the "Setup", The behaviour of each element is then analysed, and the resulting behaviour of the entire structure is computed. This computation here isperformed only after the SYSTEMCOUPLING of both the Fluid flow fluent and Static structural Analysis system is completed.

System Coupling works by integrating different solvers that are specialized in specific physics domains. These solvers are coupled through a common interface, allowing them to exchange information and communicate during the simulation. This allows for the solution of complex problems that involve the interaction of multiple physical domains. This exchange of information is enabled by suitably enabling a proper way of data transfer by defining the source and target, here in this case as FLUENT and Static structural respectively. After the successful coupling of both solvers. The software provides the results in terms of stress, deformation, and other relevant quantities, which can be used to optimize and validate the design of the structure.

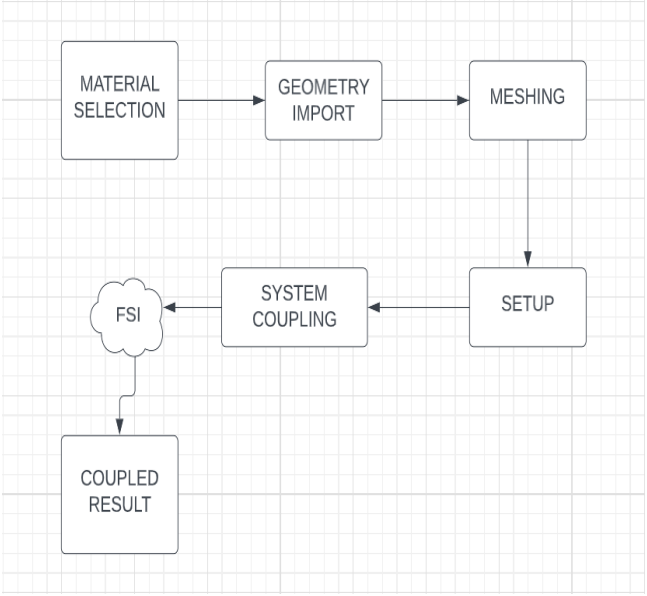

Fig. 8: Schematic representation of STATIC STRUCTURAL and Coupling approach

IV. SIMULATIONS AND RESULTS OBTAINED

The results obtained are formulated below in a tabular format along with relevant pictures to support the data.Due to its lightweight nature, the wing has been analyzed using an Aluminium alloy as the chosen material. The designed wing has been tested for four different angles of attack and the corresponding contours, plots and picturization of vortices along with Total deformation, Von-mis Stress, and Strain are shown.

A. Fluent Analysis of Diamond wedged wing at an AOA 1

High precision Fluid flow -Fluent analysis has been performed based on the above-tabulated conditions on the diamond wedged wing with an AOA of 1 degree and the results are formulated below. Required Solver settings and a detailed method of approach can be accessed by using the accompanying Research datasheet. **[17]**

Table I: Representation of primary Parameters and Settings used in the analysis

No.	Parameters	Settings
1	Type of Solver	Pressure-Based Solver
2	Energy Equation	On
3	Viscous Model	Two Equations, Standard k - E Turbulent Model
4	Fluid Medium	Air as Ideal Gas
5	Operating Altitude	1500 m
6	Operating Pressure	84643 Pascal
7	Operating Temperature	278.4 K (Correspond to the Altitude).
8	Free Stream Velocity	Mach 2.0.
9	Boundary Condition	a. Inlet as Pressure Far-Field. b. Outlet as Pressure Far-Field.
10	Angle of attack	1 Degree

Table II: Representation of Mesh size

Cells	Faces	Nodes
1337130	2712652	243010

Table III: Representation of Mesh Quality

Min Orthogonal Quality	Max Aspect Ratio
0.0013133841	463.98002

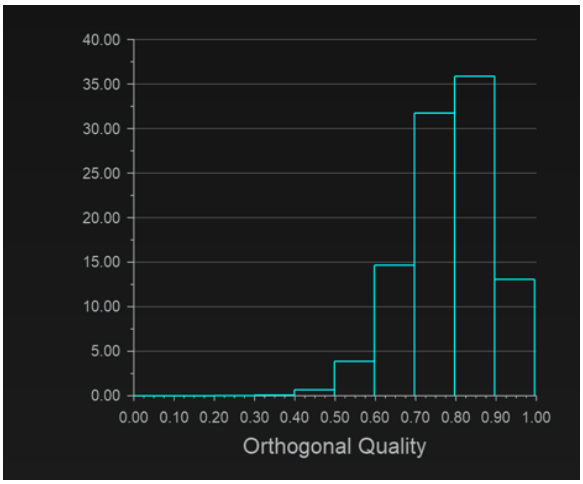

Fig. A.1: Orthogonal Quality chart showing excellent mesh

Table IV: Report definitions (Lift and Drag)

lift	3164.656 N
drag	4966.22 N

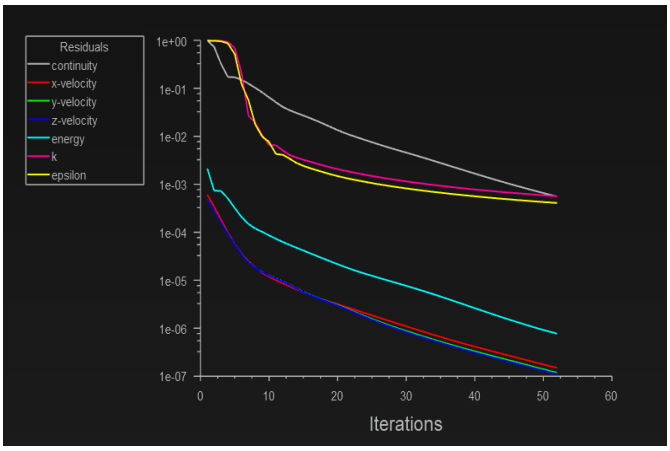

Fig. A.2: Representation of Residual plot

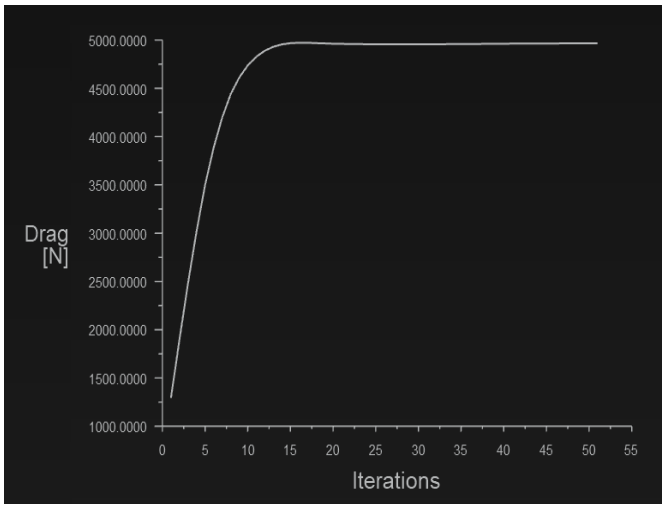

Fig. A.3: Representation of Drag plot

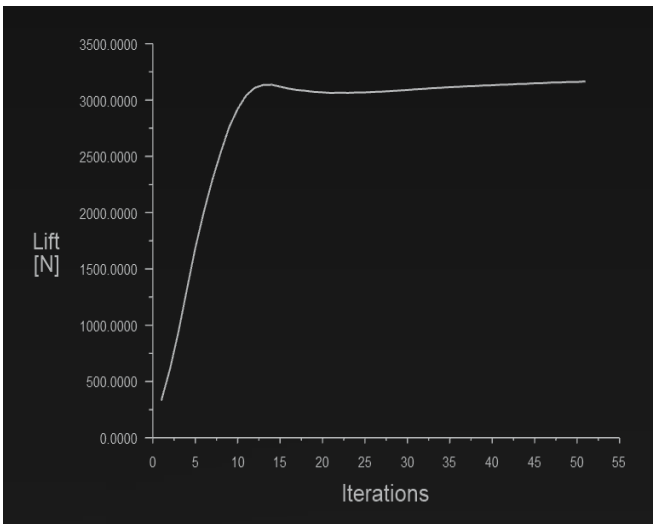

Fig. A.4: Representation of Lift plot

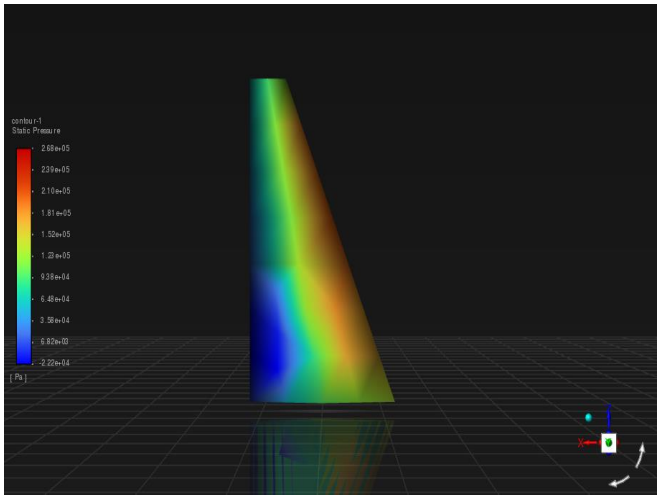

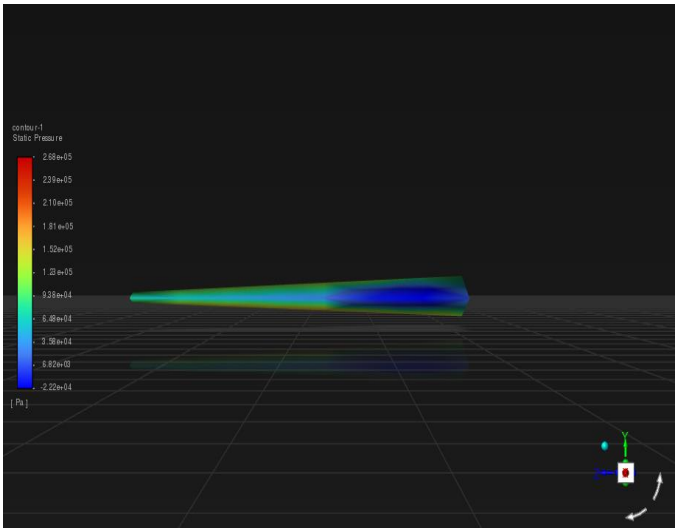

Fig. A.5: Representation of Static pressure contours

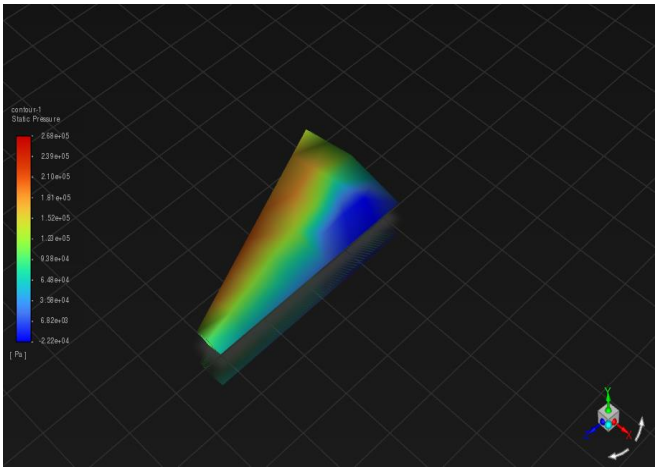

The maximum Static pressure value has been found to be 2.68e+05 Pa The minimum Static pressure value has been found to be -2.22e+04 Pa

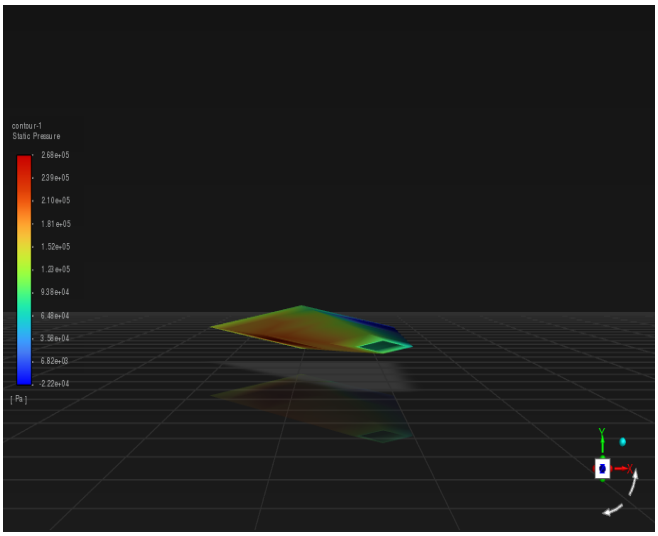

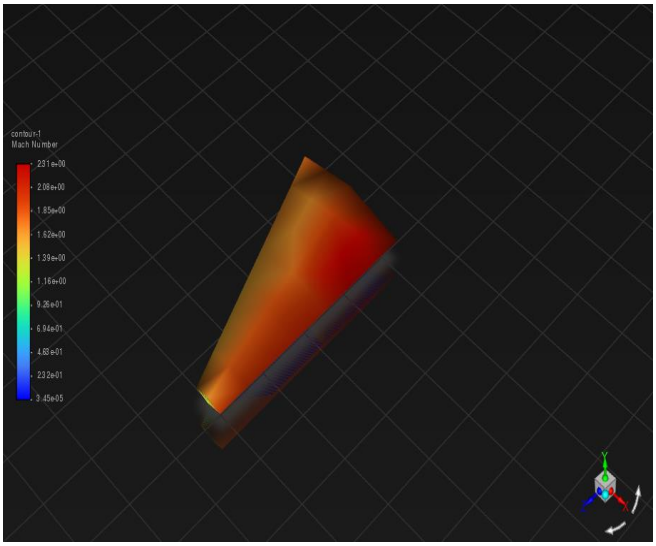

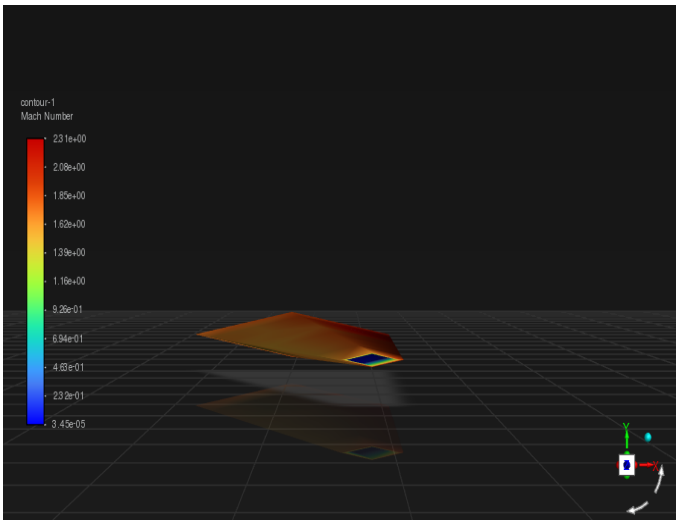

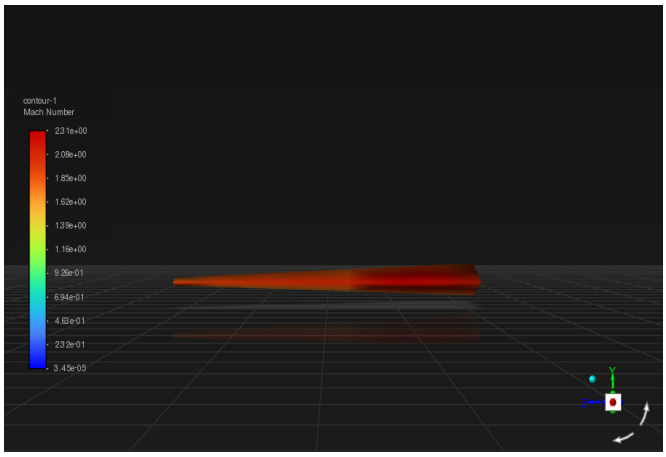

Fig. A.6: Representation of Velocity-Mach contours

The range at which the wing exhibits Mach value lies between 1.7 to 2.31 with 2.31 being the maximum value specifically at the surface of immediate contact with the penetrating air.

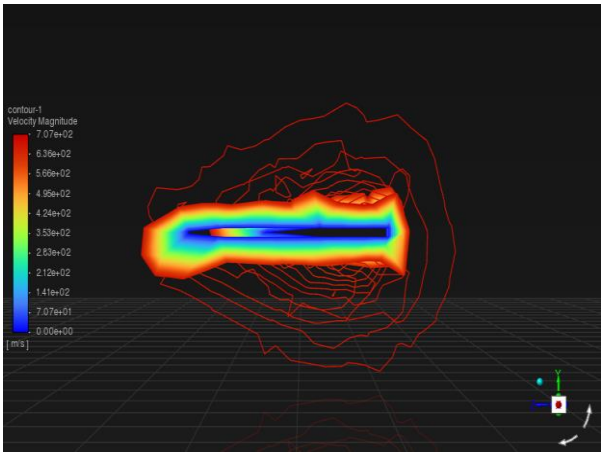

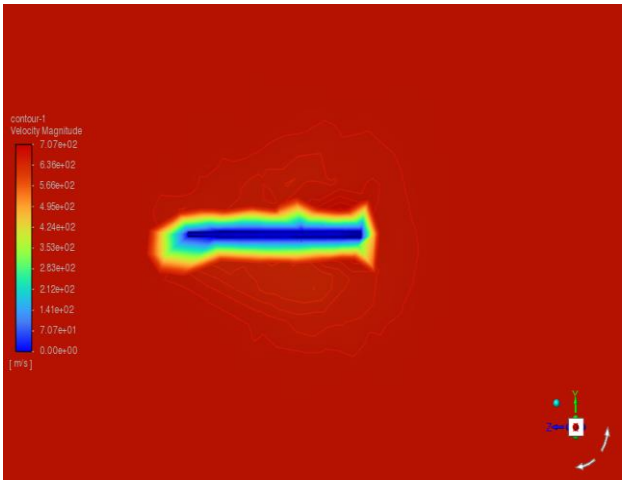

Fig. A.7: Representation of shockwaves on a plane perpendicular to the direction of fluid flow (Velocity Magnitude contour)

The distribution of velocity magnitude across the wing is clear by the cross-sectional contour view provided by Fig A.7. It shows that the circumferential area of the wing has a maximum velocity of **707 m/s** and the hollow region in the inside is where the minimum velocity of fluid flow is obtained with **0 m/s**

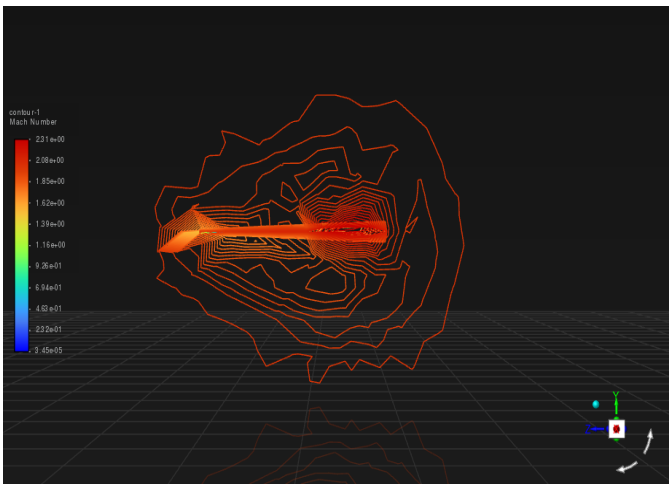

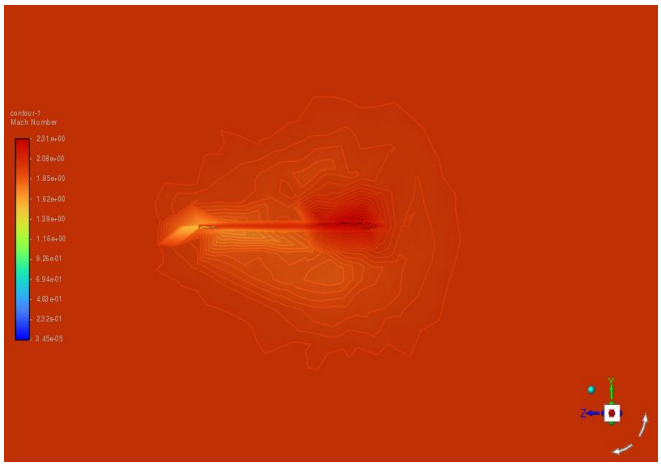

Fig. A.8: Representation of shockwaves on a plane perpendicular to the direction of flow of fluid (Mach contour)

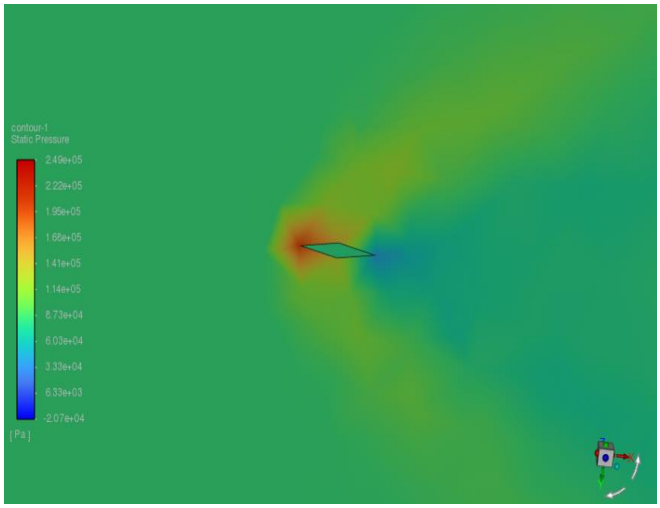

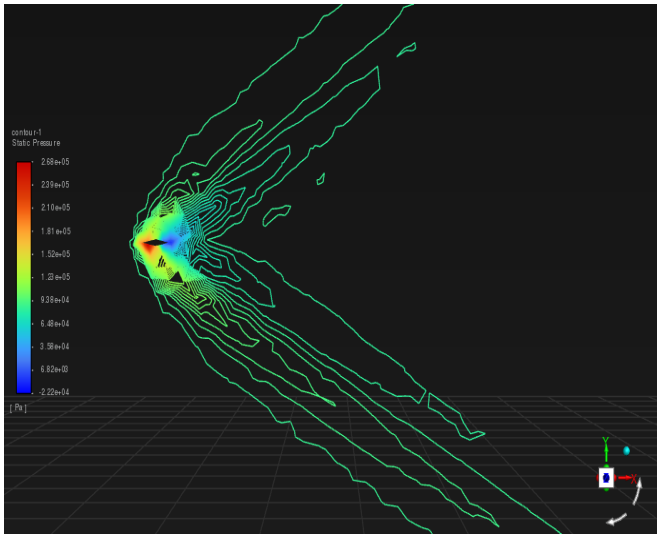

Fig. A.9: Representation of propagation of filled/unfilled shockwaves around the Diamond wedge airfoil (Static pressure contour)

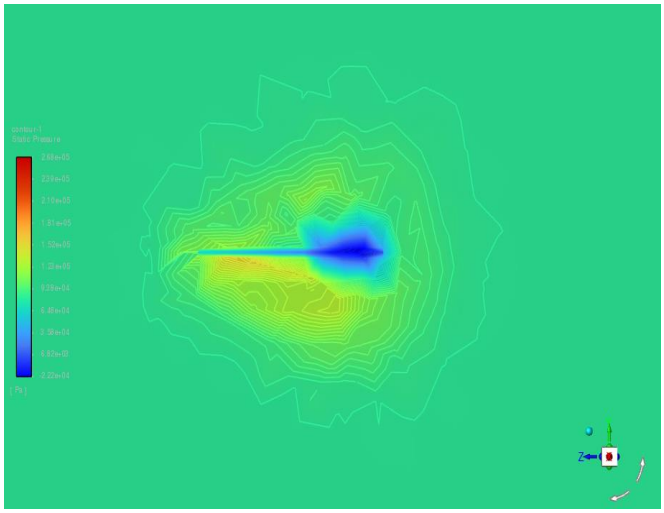

Fig. A.10: Representation of shockwaves on a plane perpendicular to the direction of flow of fluid (Static pressure contour)

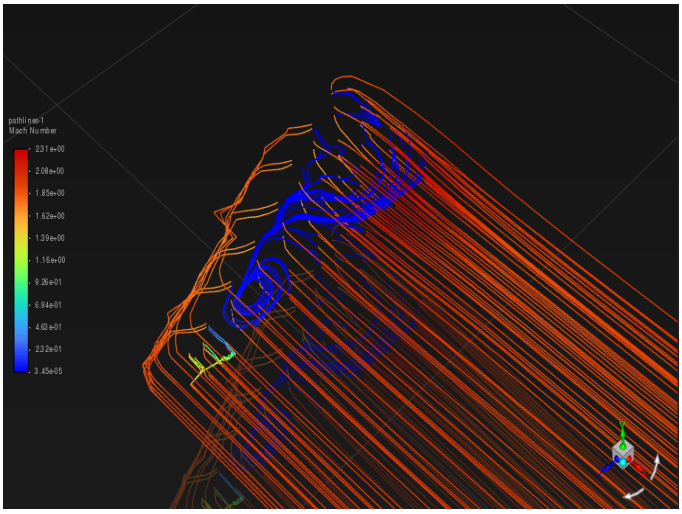

Fig. A:11: Representation of pathlines indicating the vortices

The swirling movement of considerable path lines indicates the vortex generation with Higher Mach as represented which in turn induces the practical phenomenon of instability and thus leads to flutter/Self-excited oscillation.

B. Structural Analysis of Diamond wedged wing at an AOA of 1°

UNITS

Unit System	Metric (m, kg, N, s, V, A) Degrees rad/s Celsius
Angle	Degrees
Rotational Velocity	rad/s
Temperature	Celsius

Fig. B.1: Representation of units

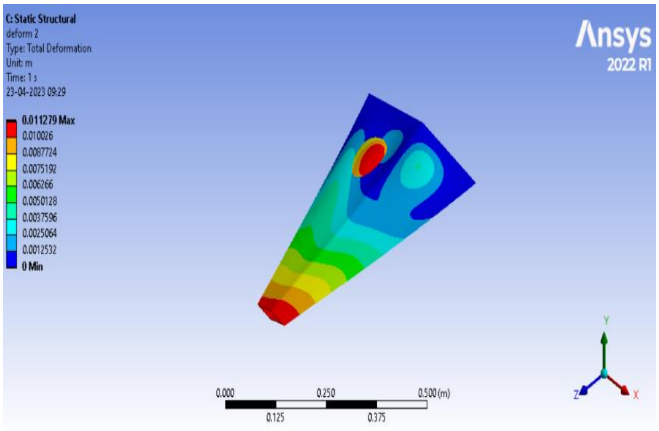

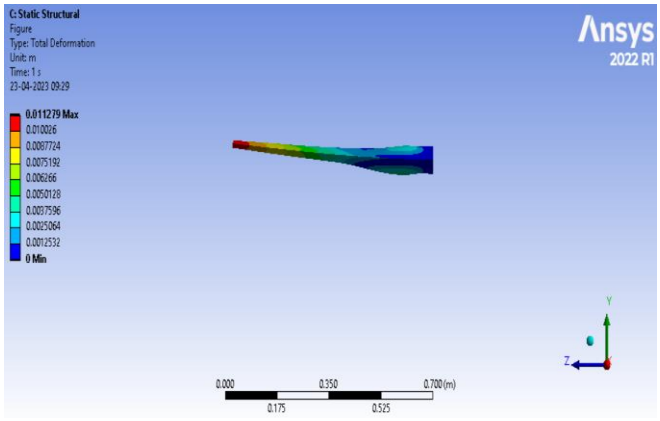

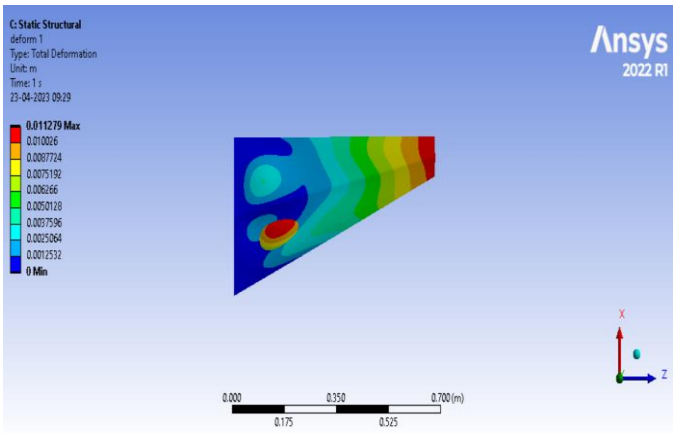

Fig. B.2: Representation of total deformation

The maximum value of Total deformation was found to be **0.011279 m** and is vividly seen in the wing tip as the wing tip acts as the free end of a supposed cantilever beam for instance which is more susceptible to deformation. The minimum value of Total deformation is **0 m** at the fixed part of the wing

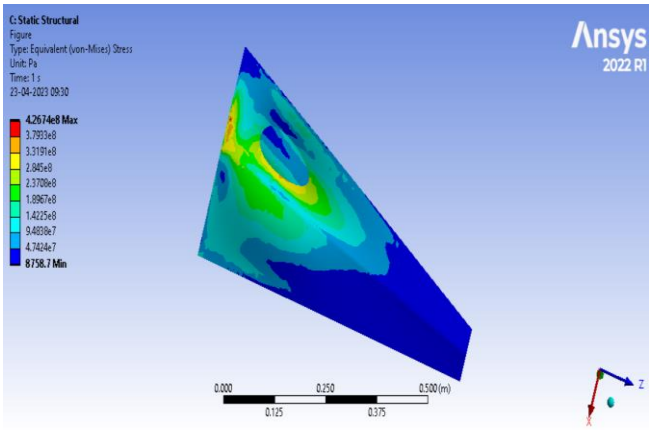

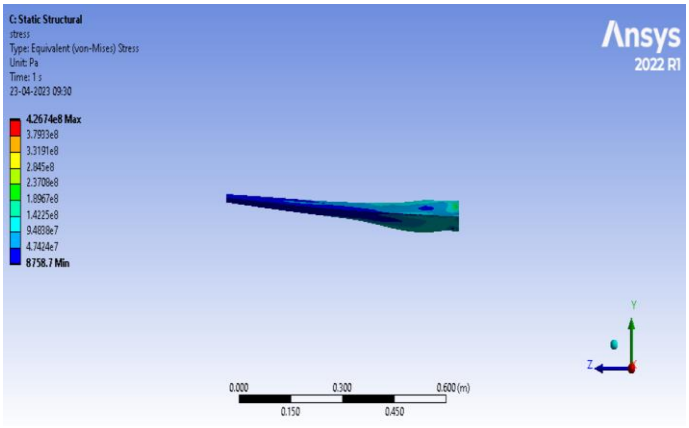

Fig. B.3: Representation of Equivalent stress

The maximum value of Von-mises stress is found to be **4.2674e08 Pa** whereas the minimum value is found to be **8758.7 Pa**

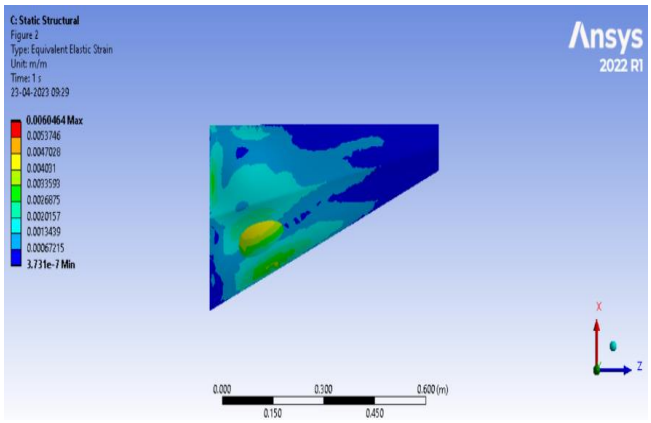

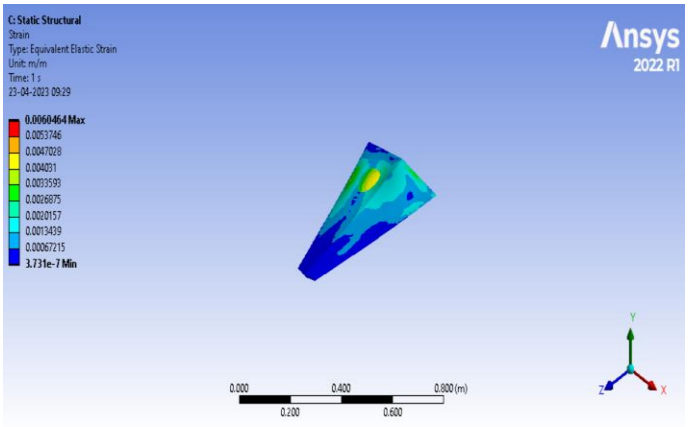

Fig. B.4: Representation of Equivalent elastic strain

The maximum value of Strain is found to be **0.00604064** and the minimum value is in the order of e-7 with a precise value of **3.731e-7**

C. Fluent Analysis of Diamond wedged wing at an AOA 2°

High precision Fluid flow -Fluent analysis has been performed based on the above-tabulated conditions on the diamond wedged wing with an AOA of 2 degrees and the results are formulated below. Required Solver settings and a detailed method of approach can be accessed by using the accompanying Research datasheet.

Table I: Representation of primary Parameters and Settings used in the analysis

No.	Parameters	Settings
1	Type of Solver	Pressure-Based Solver
2	Energy Equation	On
3	Viscous Model	Two Equations, Standard k - E Turbulent Model
4	Fluid Medium	Air as Ideal Gas
5	Operating Altitude	1500 m
6	Operating Pressure	84643 Pascal
7	Operating Temperature	278.4 K (Correspond to the Altitude).
8	Free Stream Velocity	Mach 2.0.
9	Boundary Condition	a. Inlet as Pressure Far-Field. b. Outlet as Pressure Far-Field.
10	Angle of attack	2 Degrees

Table II: Representation of Mesh size

Cells	Faces	Nodes
1337130	2712652	243010

Table III: Representation of Mesh Quality

Name	Type	Min Orthogonal Quality	Max Aspect Ratio
farfield	Tet Cell	0.0013133841	463.98002

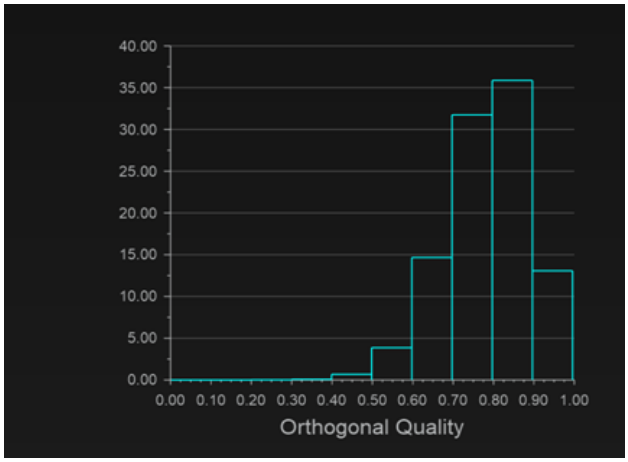

Fig. C.1: Orthogonal Quality chart showing excellent mesh

Table IV: Report definitions (Lift and Drag)

drag	4998.463 N
lift	6376.365 N

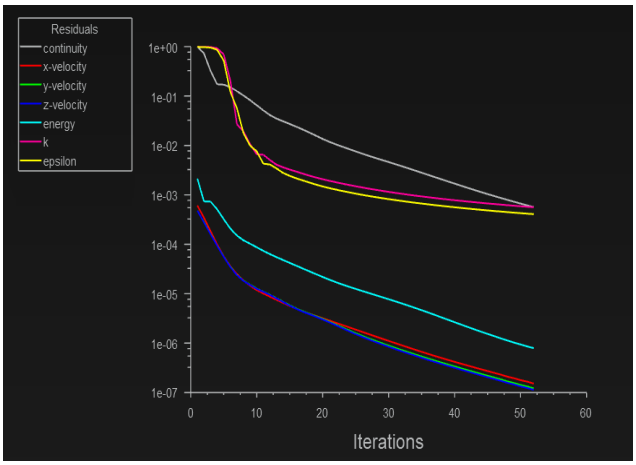

Fig. C.2: Representation of Residual plot

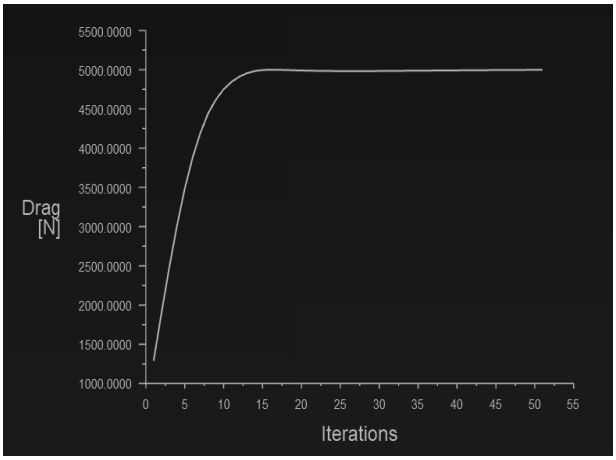

Fig. C.3: Representation of Drag plot

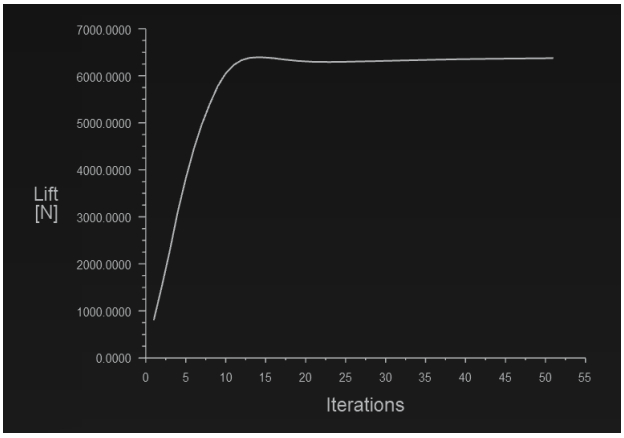

Fig. C.4: Representation of Lift plot

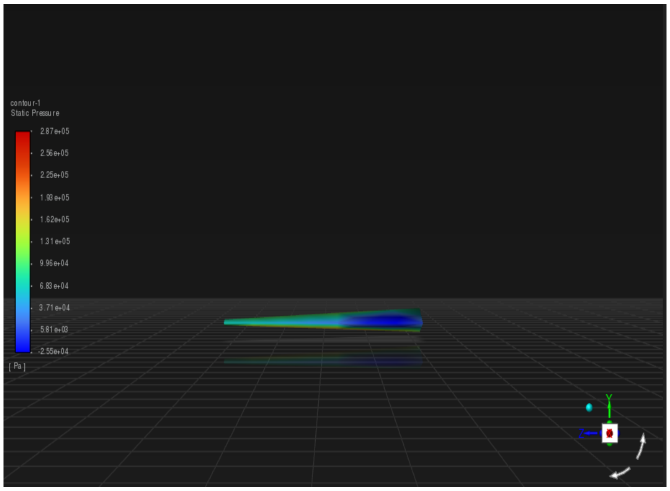

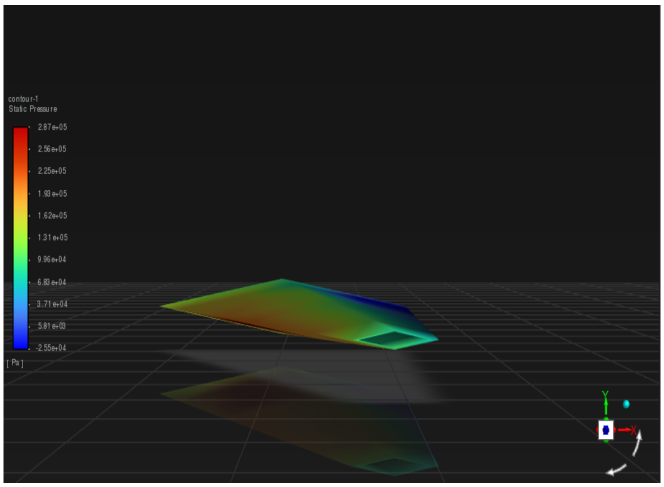

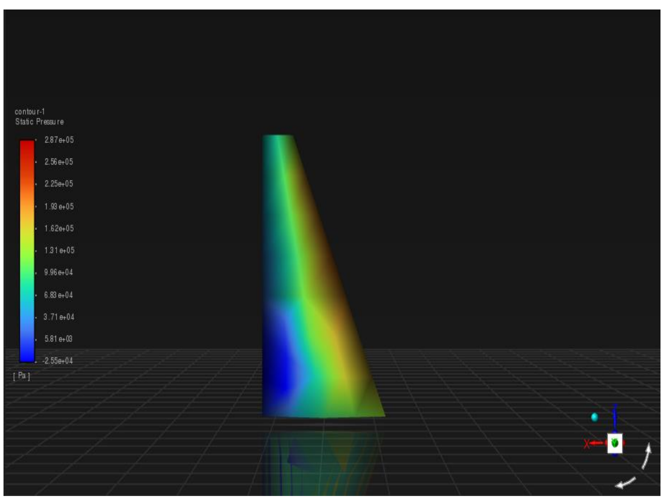

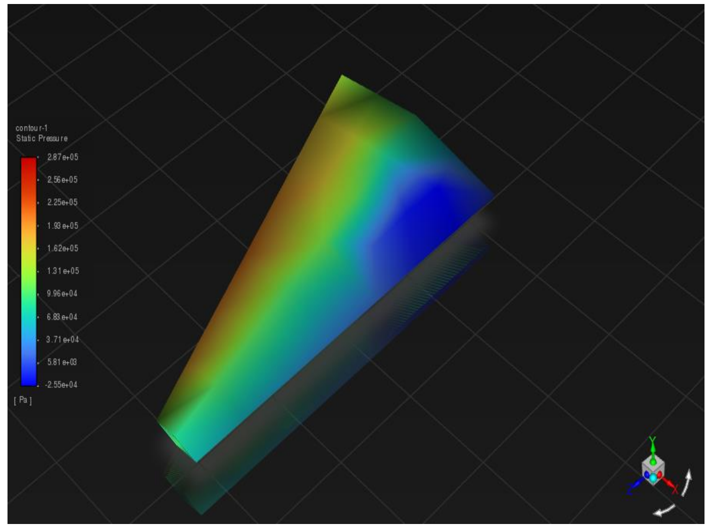

Fig. C.5: Representation of Static pressure contour

The maximum Static pressure value has been found to be 2.87e+05 Pa The minimum Static pressure value has been found to be -2.55e+04 Pa

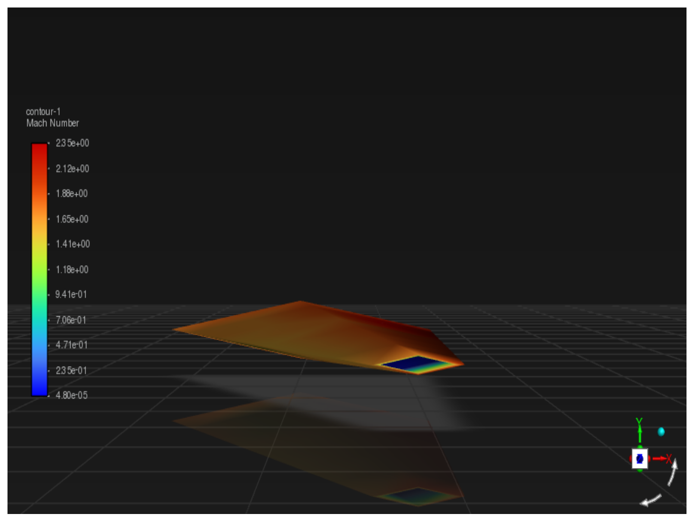

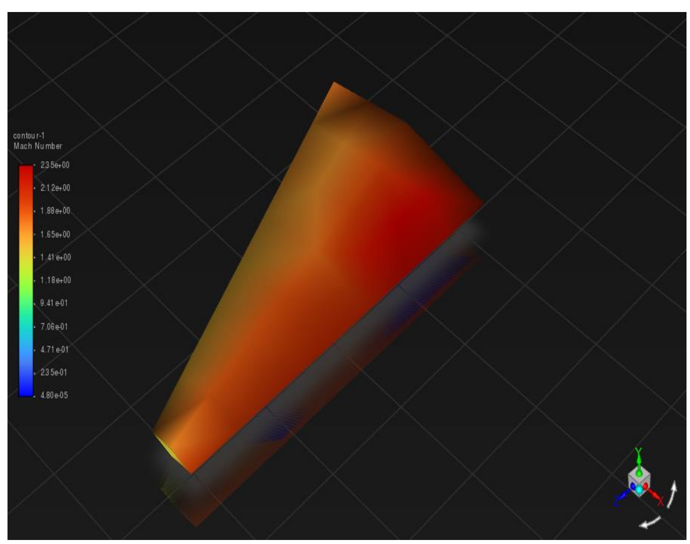

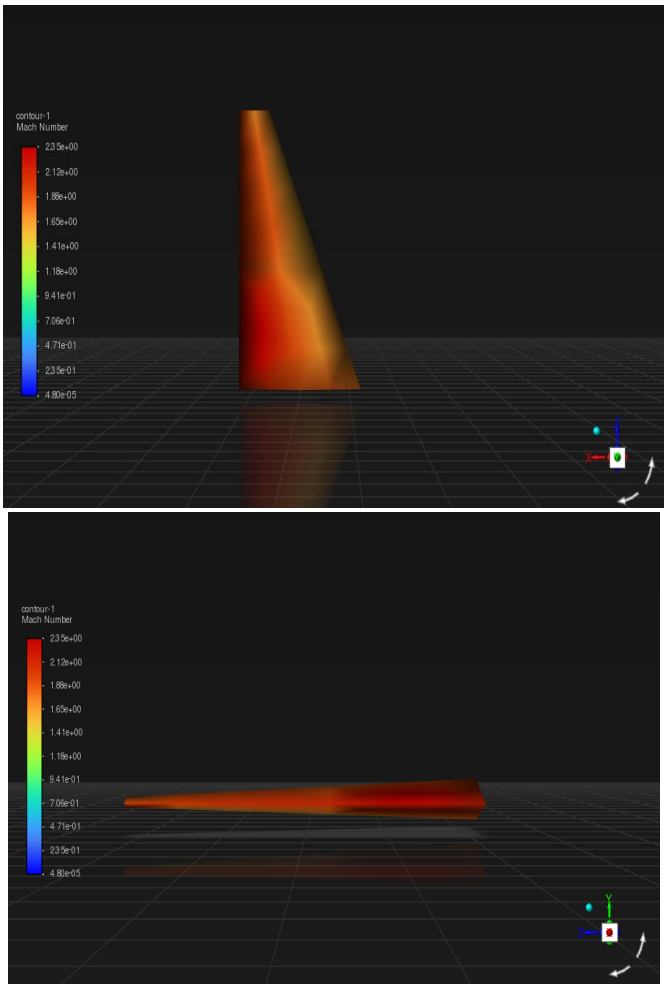

Fig. C.6: Representation of Velocity-Mach contours

The range at which the wing exhibits Mach value lies between 1.8 to 2.35 with 2.35 being the maximum value specifically at the surface of immediate contact with the penetrating air.

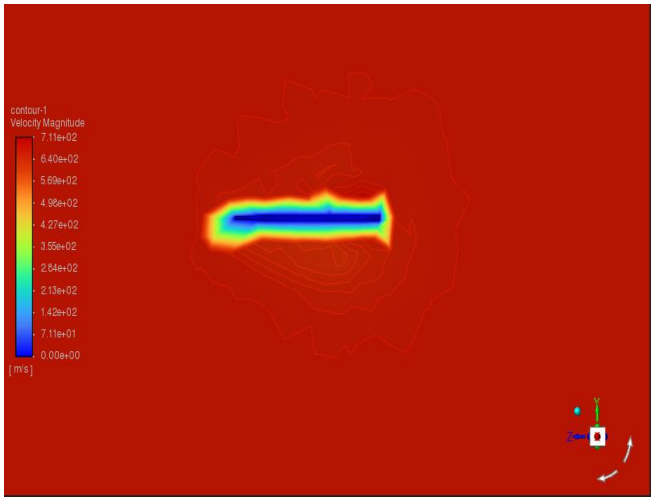

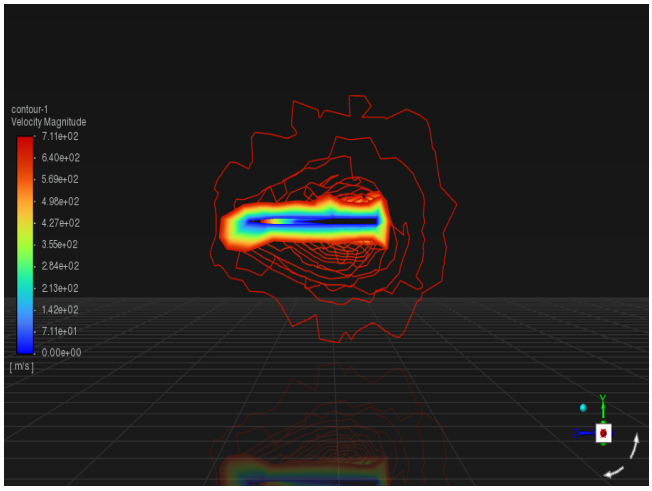

Fig. C.7: Representation of shockwaves on a plane perpendicular to the direction of fluid flow (Velocity Magnitude contour)

The distribution of velocity magnitude across the wing is clear by the cross-sectional contour view provided by Fig C.7. It shows that the circumferential area of the wing has a maximum velocity of **711 m/s** and the hollow region in the inside is where the minimum velocity of fluid flow is obtained with **0 m/s**

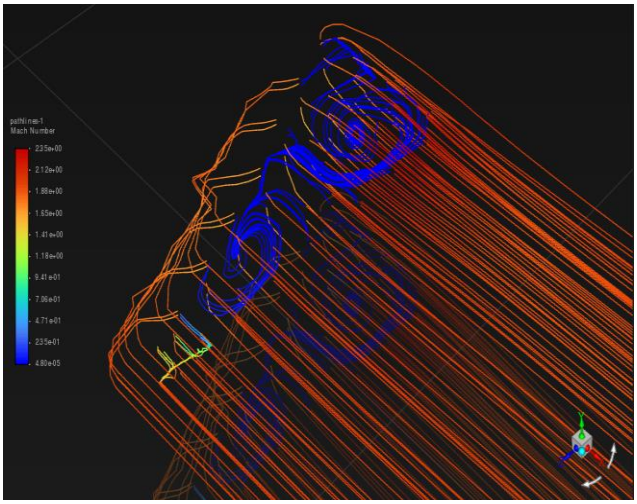

Fig. C.8: Representation of pathlines indicating the vortices

The swirling movement of considerable pathlines indicates the vortex generation with Higher Mach as represented which in turn induces the practical phenomenon of instability and thus leads to flutter/Self-excited oscillation. The vortices induced here are of higher intensity with the swirling movement covering larger regions as compared to the vortices induced in the same wing with AOA 1 degree.

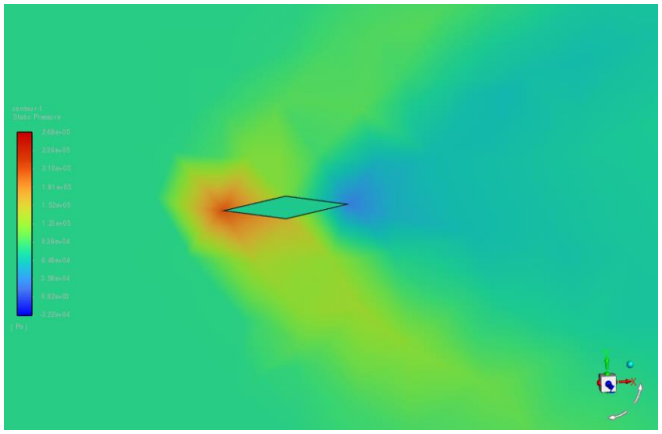

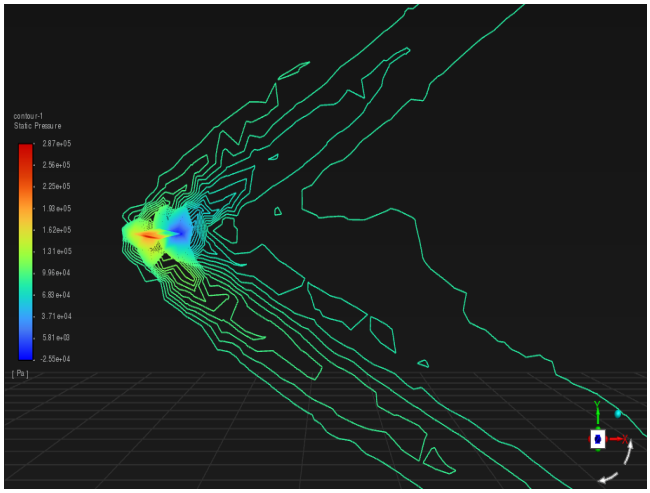

Fig. C.9: Representation of propagation of filled/unfilled shockwaves around the Diamond wedge airfoil (Static pressure contour)

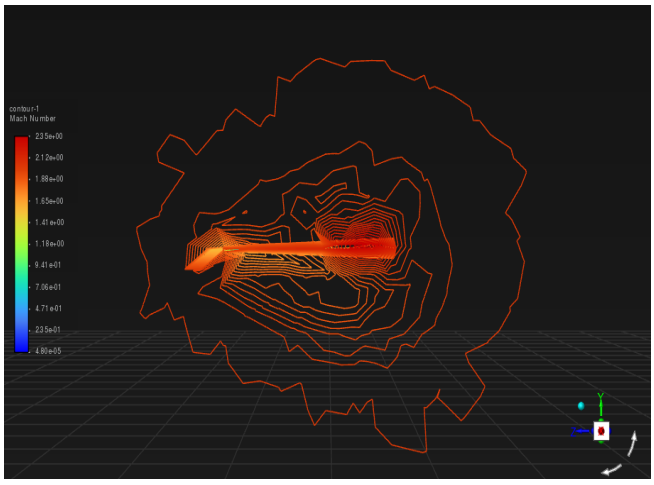

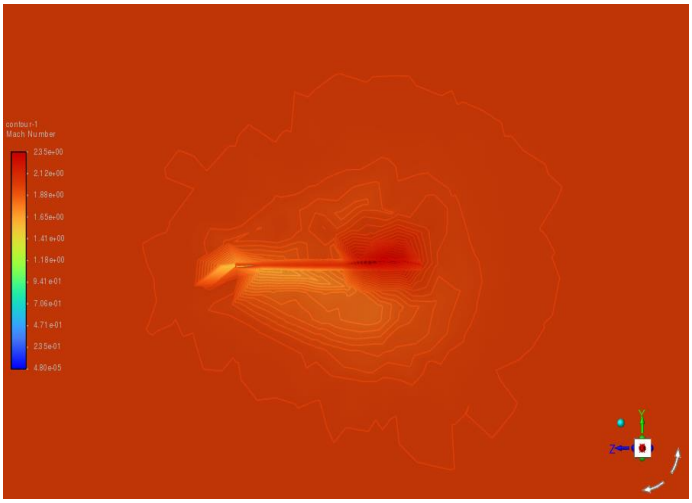

Fig. C.10: Representation of shockwaves on a plane perpendicular to the direction of fluid flow (Velocity-Mach contour)

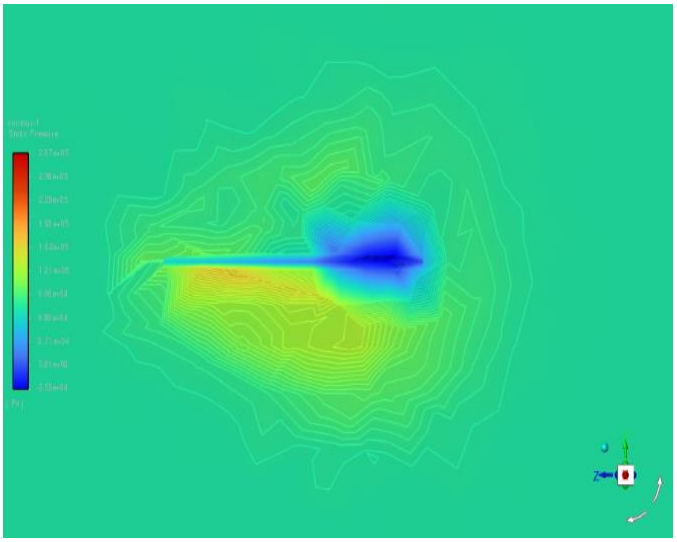

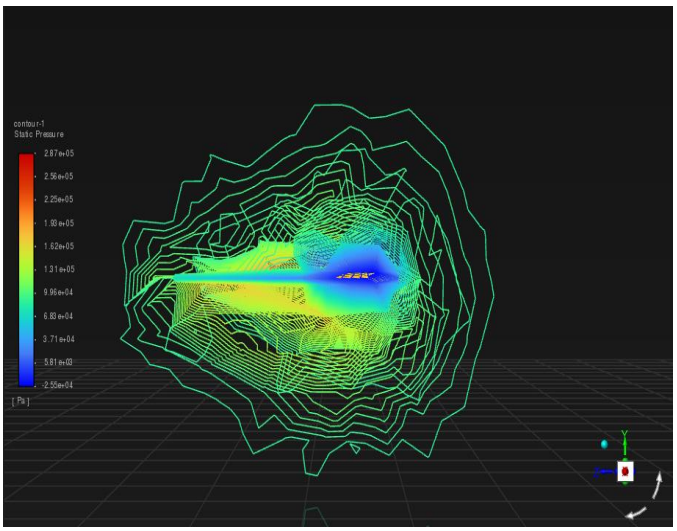

Fig. C.11: Representation of shockwaves on a plane perpendicular to the direction of flow of fluid (Static pressure contour)

D. Structural Analysis of Diamond wedged wing at an AOA 2°

UNITS	
Unit System	Metric (m, kg, N, s, V, A) Degrees rad/s Celsius
Angle	Degrees
Rotational Velocity	rad/s
Temperature	Celsius

Fig. D1: Representation of units

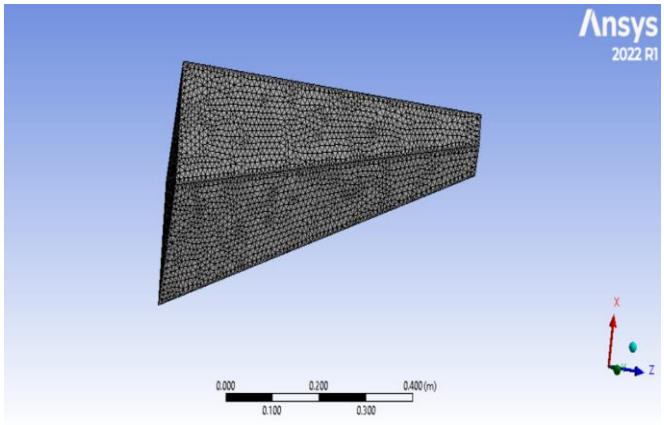

Fig. D.2: Representation of Mesh

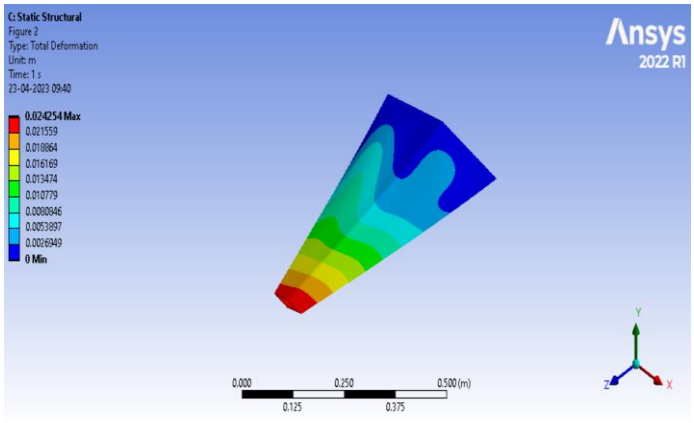

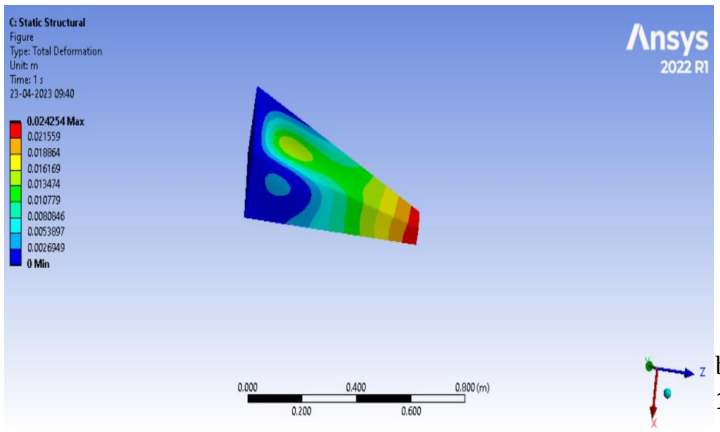

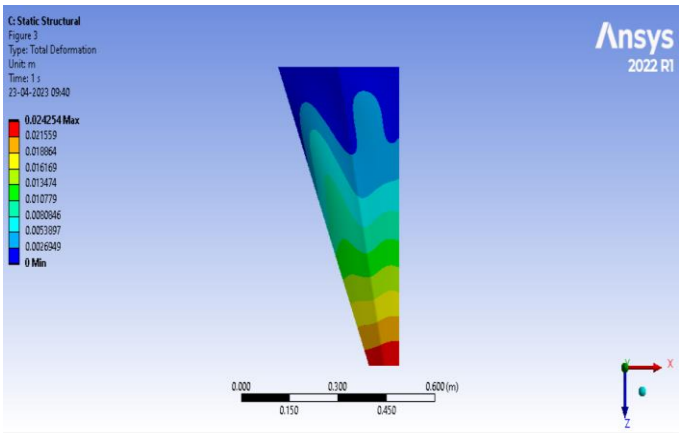

Fig. D.3: Representation of total deformation

The maximum value of Total deformation was found to be **0.024254 m** and is vividly seen in the wing tip as the wing tip acts as the free end of a supposed cantilever beam for instance which is more susceptible to deformation. The minimum value of Total deformation is **0 m** at the fixed part of the wing

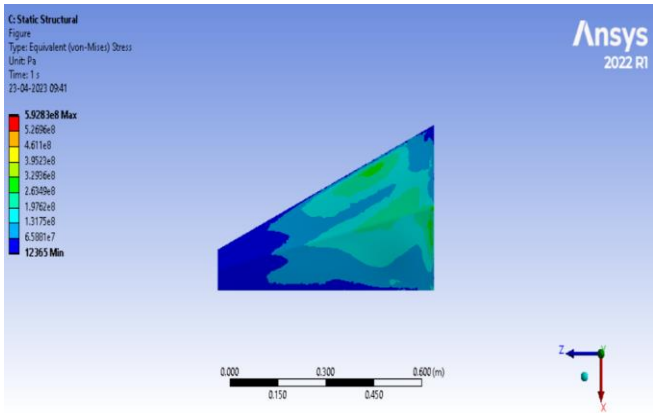

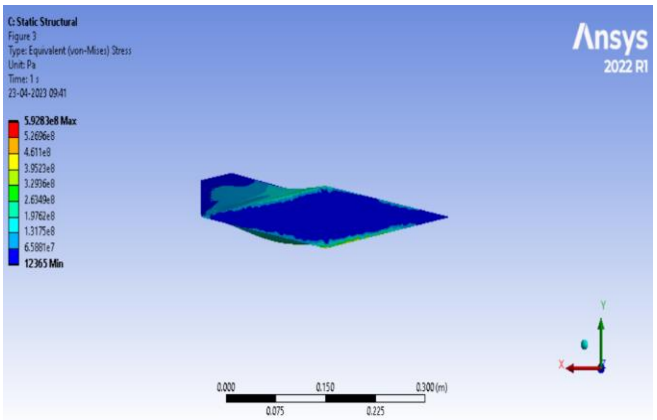

Fig. D.4: Representation of Equivalent stress

The maximum value of Von-mises stress is found to be **5.9283e08 Pa** whereas the minimum value is found to be **12365 Pa**

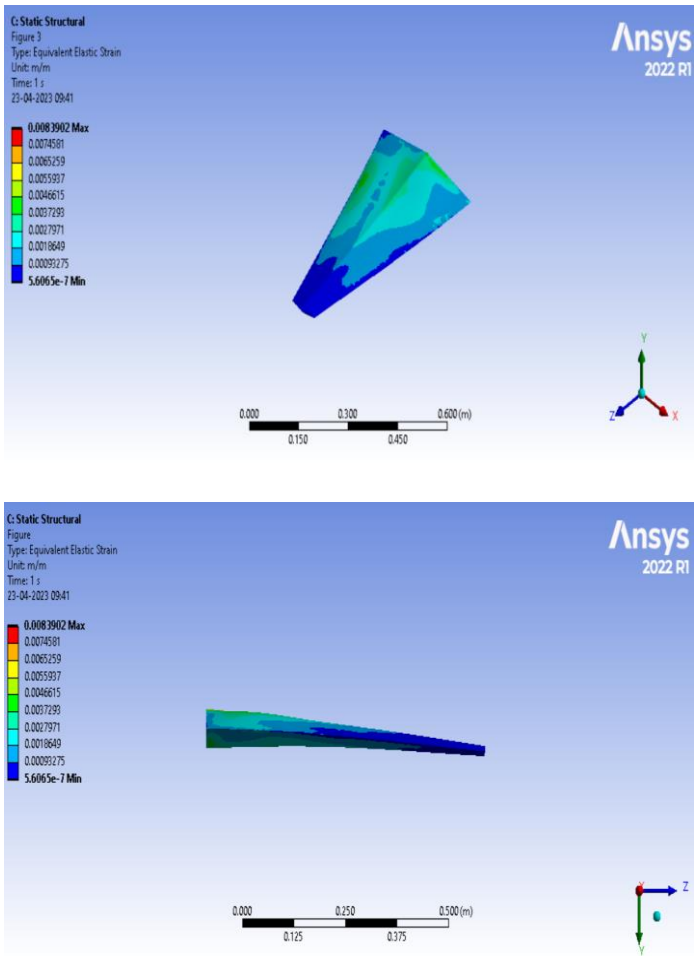

Fig. D.5: Representation of Equivalent elastic strain

The maximum value of Strain is found to be **0.0083902** and the minimum value is in the order of e-7 with a precise value of **5.6065e-7**

E. Fluent Analysis of wing 2 at an AOA 1°

High precision Fluid flow -Fluent analysis has been performed based on the above-tabulated conditions on the Customised wing 2 with an AOA of 1 degree and the results are formulated below. Required Solver settings and a detailed method of approach can be accessed by using the accompanying Research datasheet.

Table I: Representation of primary Parameters and Settings used in the analysis

No.	Parameters	Settings
1	Type of Solver	Pressure-Based Solver
2	Energy Equation	On
3	Viscous Model	Two Equations, Standard k - E Turbulent Model
4	Fluid Medium	Air as Ideal Gas
5	Operating Altitude	1500 m
6	Operating Pressure	84643 Pascal
7	Operating Temperature	278.4 K (Correspond to the Altitude).
8	Free Stream Velocity	Mach 2.0.
9	Boundary Condition	a. Inlet as Pressure Far-Field. b. Outlet as Pressure Far-Field.
10	Angle of attack	1 Degree

Table II: Representation of Mesh size

Cells	Faces	Nodes
1717046	3483859	312346

Table III: Representation of Mesh Quality

Name	Type	Min Orthogonal Quality	Max Aspect Ratio
farfield	TetCell	0.00059586577	466.67949

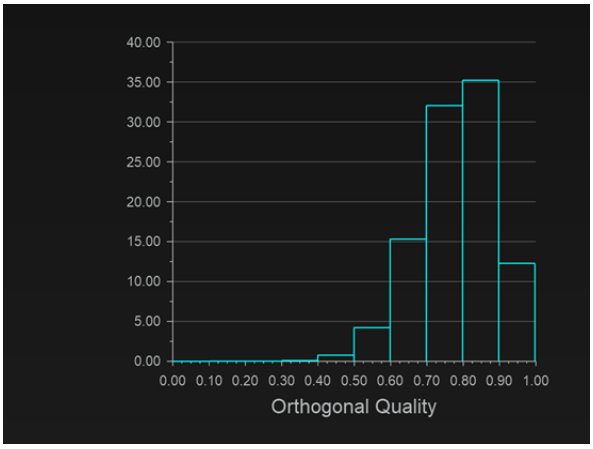

Fig.E.1: Orthogonal Quality chart showing excellent mesh

Table IV: Report definitions (Lift and Drag)

drag	13789.87 N
lift	4313.597 N

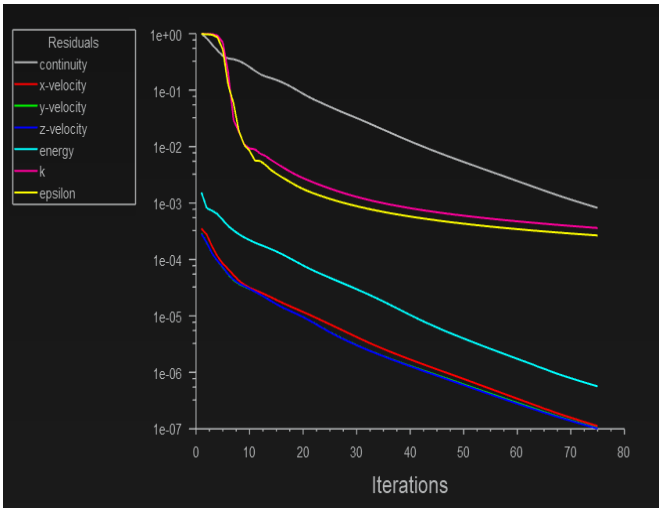

Fig.E.2: Representation of Residual plot

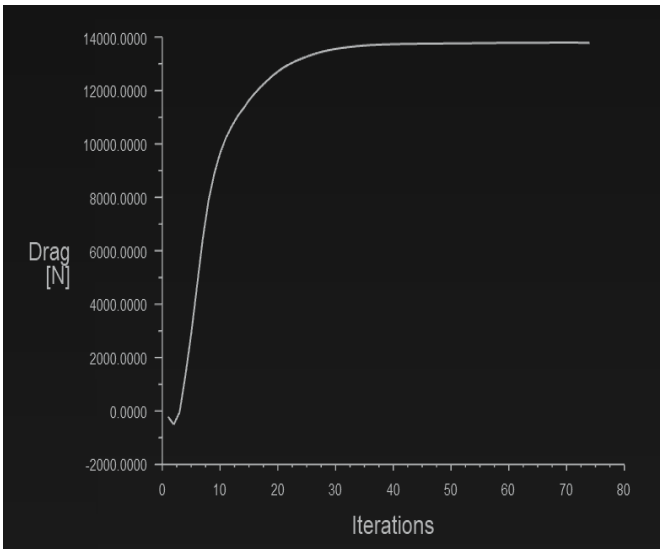

Fig.E.3: Representation of Drag plot

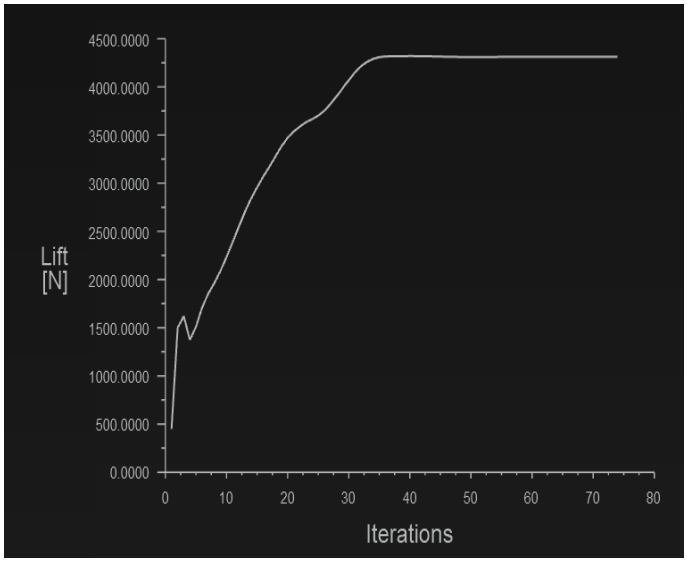

Fig.E.4: Representation of Lift plot

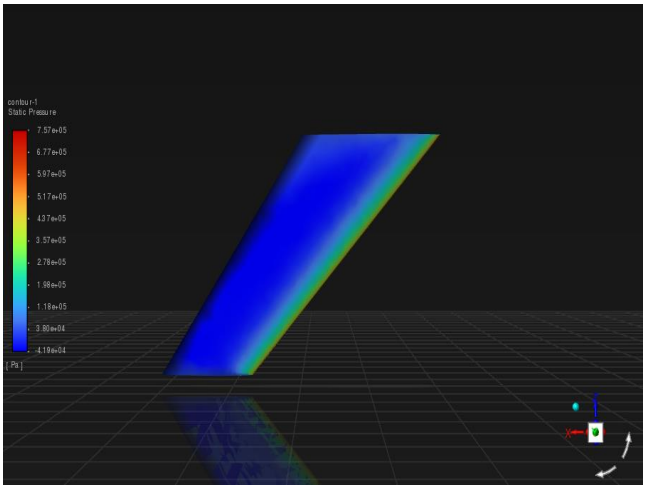

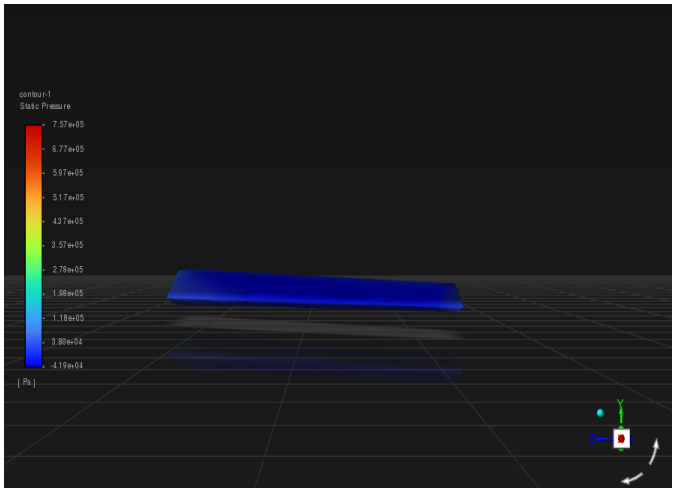

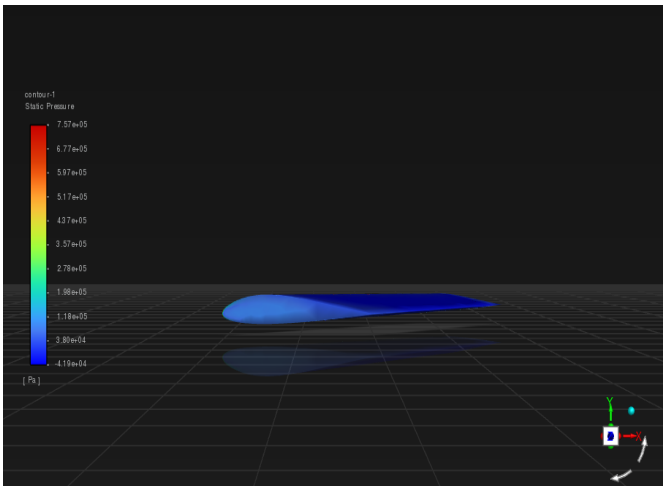

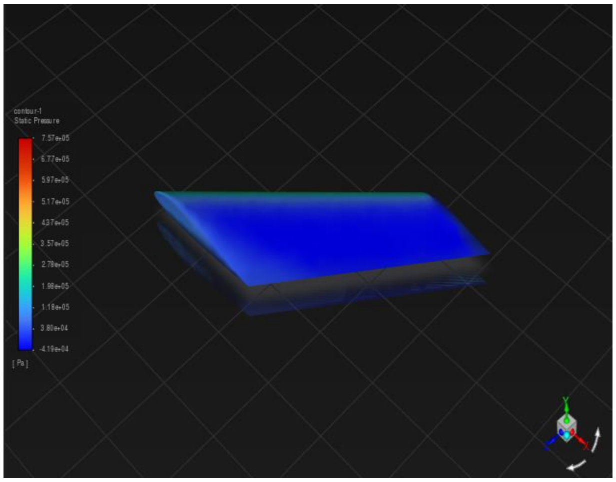

Fig.E.5: Representation of Static pressure contours

The maximum Static pressure value has been found to be 7.57e+05 Pa. The minimum Static pressure value has been found to be -4.19e+04 Pa

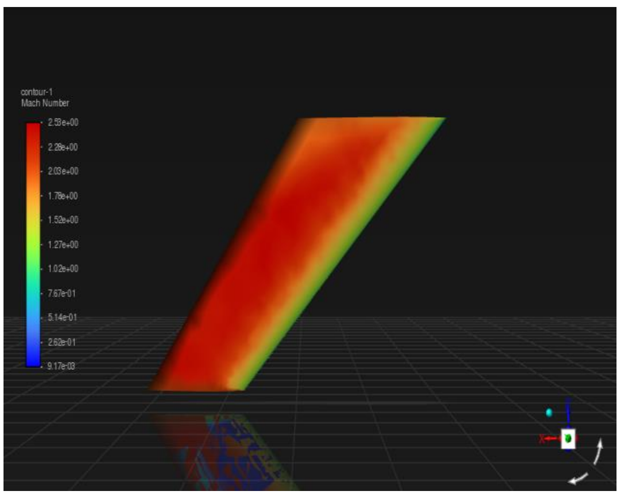

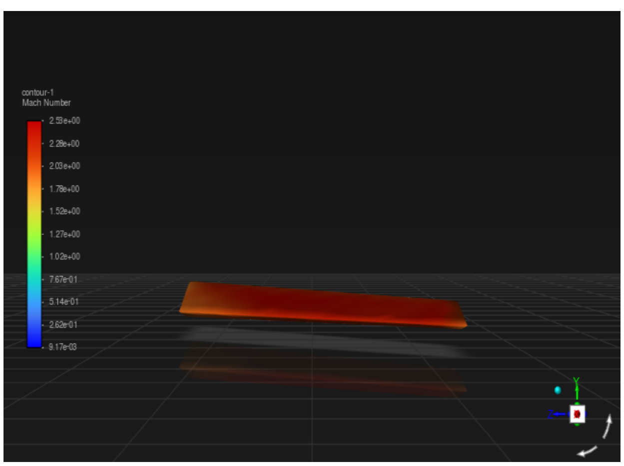

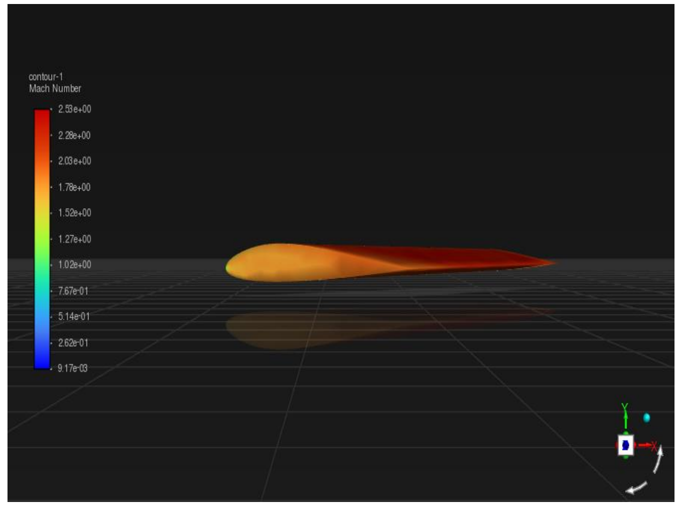

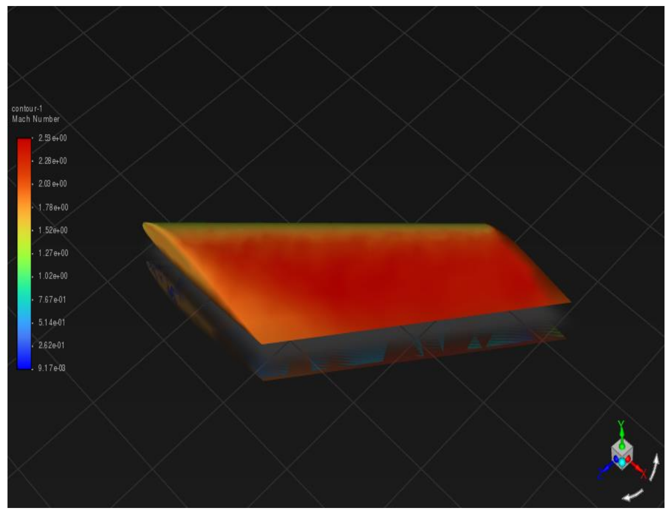

Fig.E.6: Representation of Velocity-Mach contours

The range at which the wing exhibits Mach value lies between 1.2 to 2.53 with 2.53 being the maximum value specifically at the surface of immediate contact with the penetrating air.

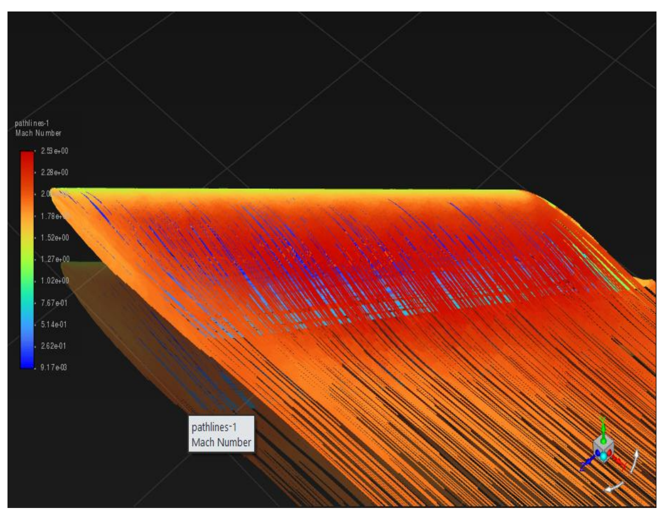

Fig.E.7: Representation of pathlines

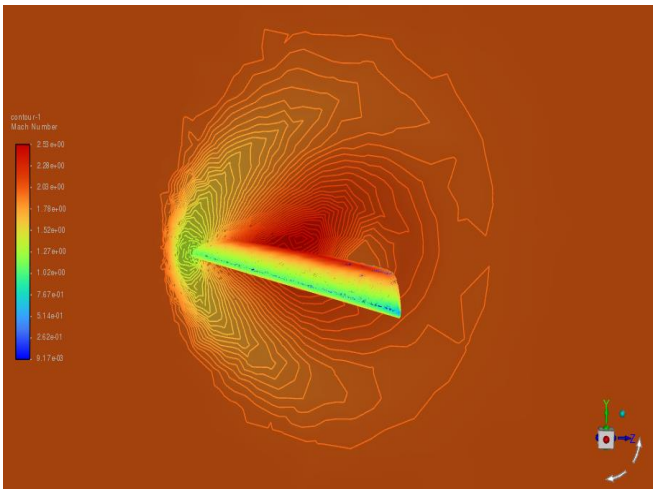

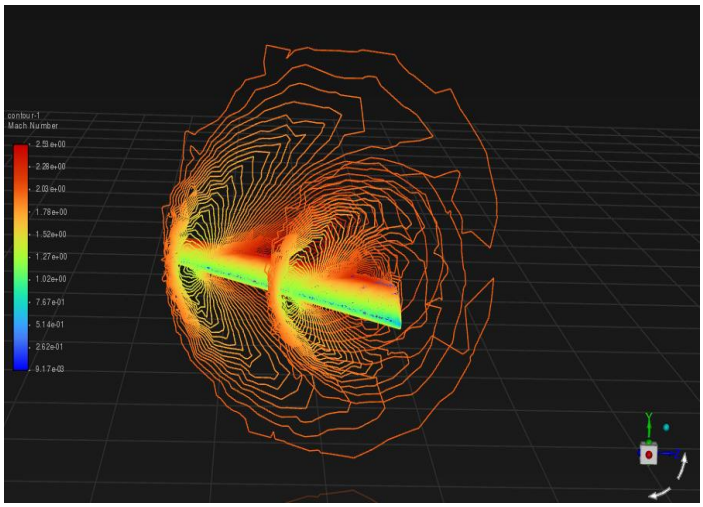

Fig.E.8: Representation of shockwaves on a plane perpendicular to the direction of fluid flow (Velocity Mach contour)

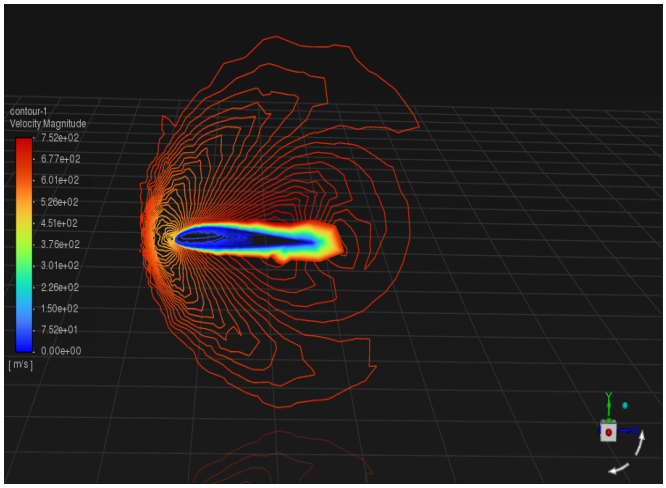

Fig.E.9: Representation of shockwaves on a plane perpendicular to the direction of fluid flow (Velocity Magnitude contour)

The distribution of velocity magnitude across the wing is clear by the cross-sectional contour view provided by Fig E.9. It shows that the circumferential area of the wing has a maximum velocity of **707 m/s** and the hollow region in the inside is where the minimum velocity of fluid flow is obtained with **0 m/s**

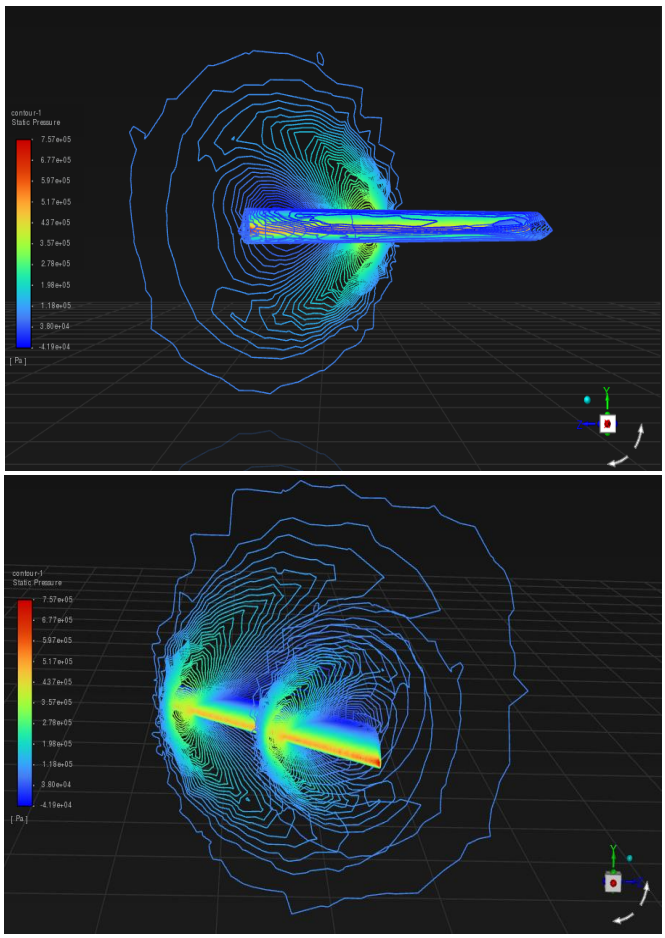

Fig. E.10: Representation of shockwaves on a plane perpendicular to the direction of fluid flow (Static Pressure contour)

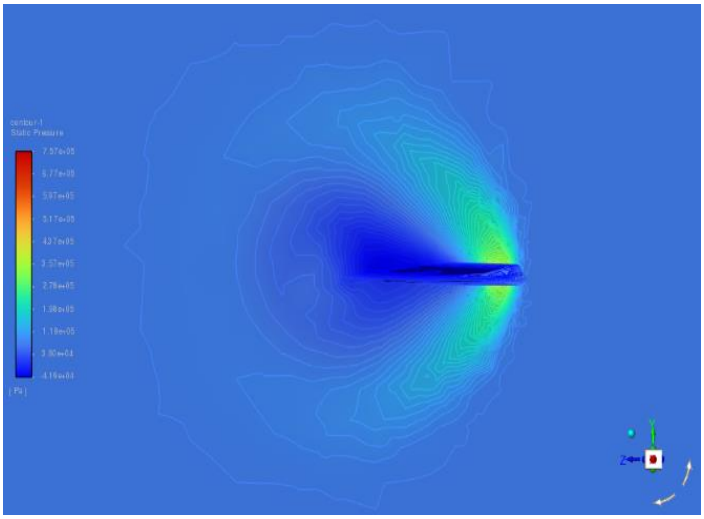

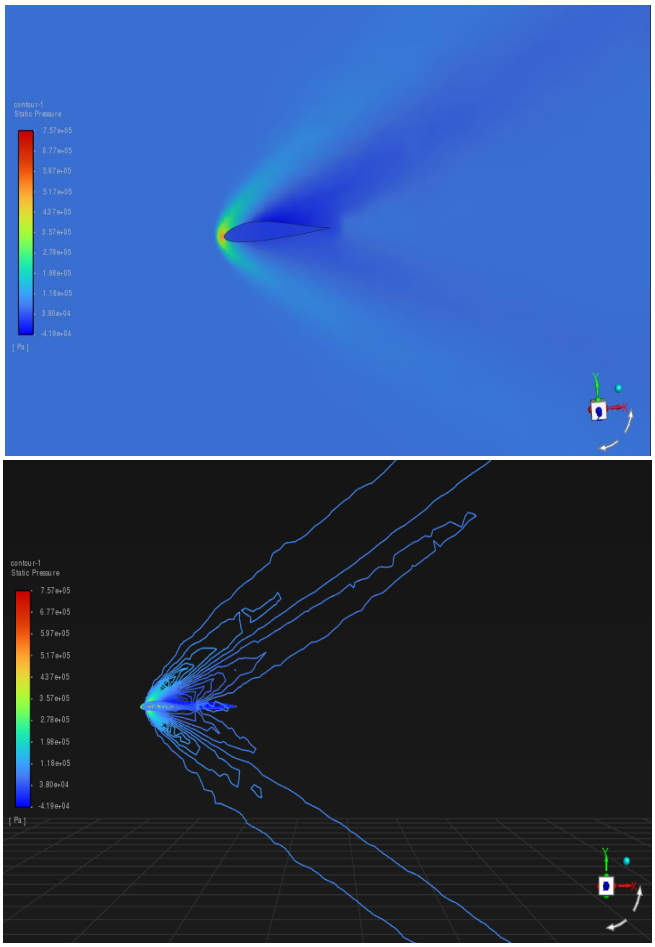

Fig.E.11: Representation of propagation of filled/unfilled shockwaves around the airfoil (Static pressure contour)

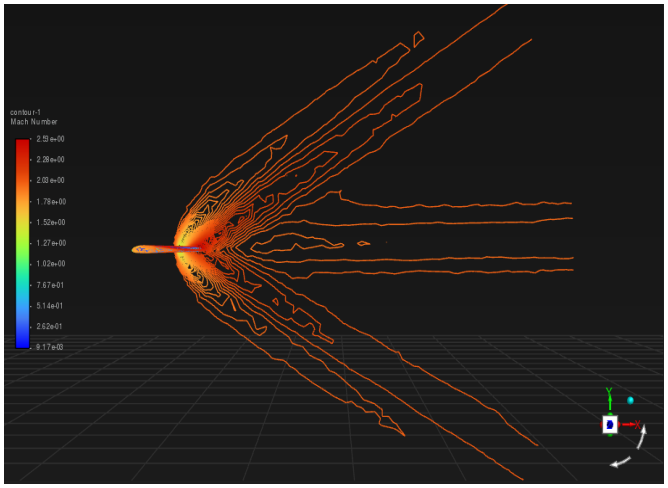

Fig.E:12: Representation of propagation of unfilled shockwaves around the airfoil (Velocity-Mach contour)

F. Structural Analysis of wing 2 at an AOA 1°

UNITS	
Unit System	Metric (m, kg, N, s, V, A) Degrees rad/s Celsius
Angle	Degrees
Rotational Velocity	rad/s
Temperature	Celsius

Fig.F.1: Representation of units

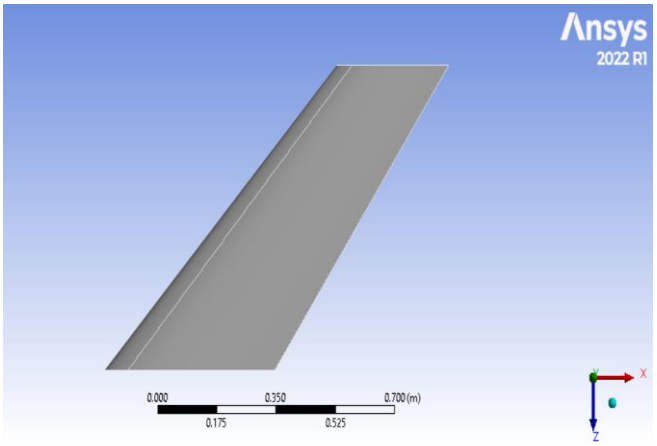

Fig.F.2: Representation of geometry

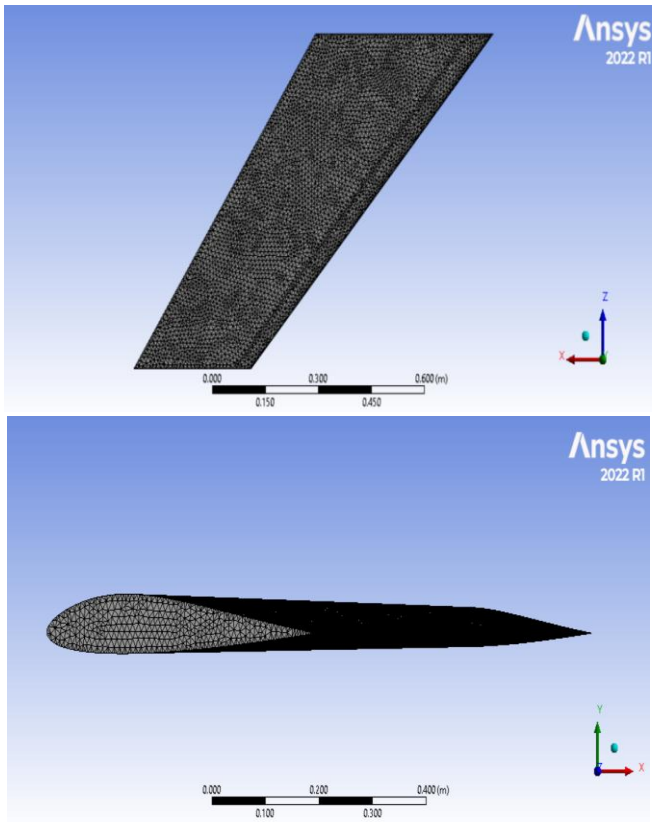

Fig.F.3: Representation of Mesh

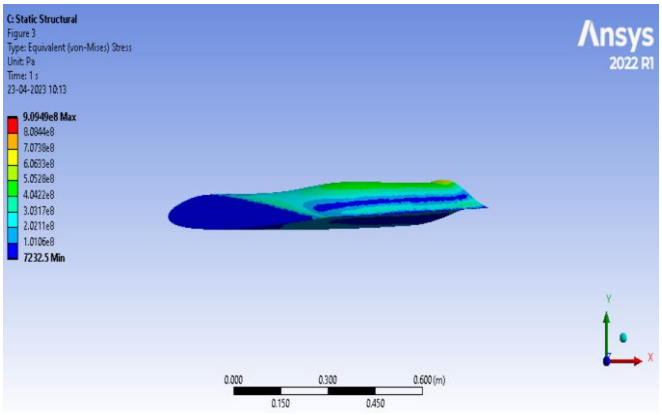

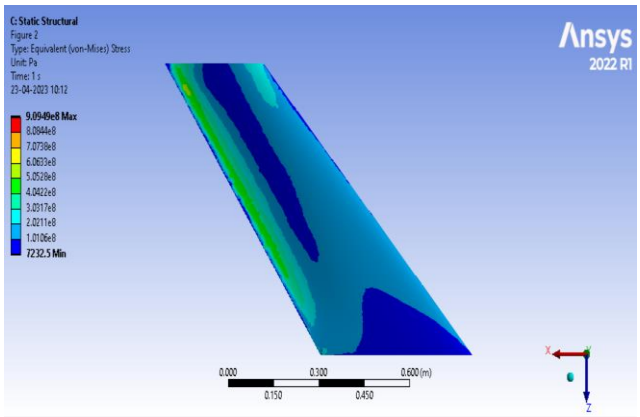

Fig.F.4: Representation of Equivalent stress

The maximum value of Von-mises stress is found to be **9.0949e08 Pa** whereas the minimum value is found to be **7232.5 Pa**

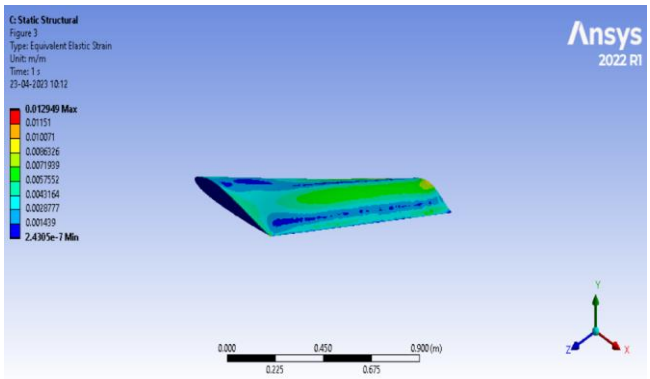

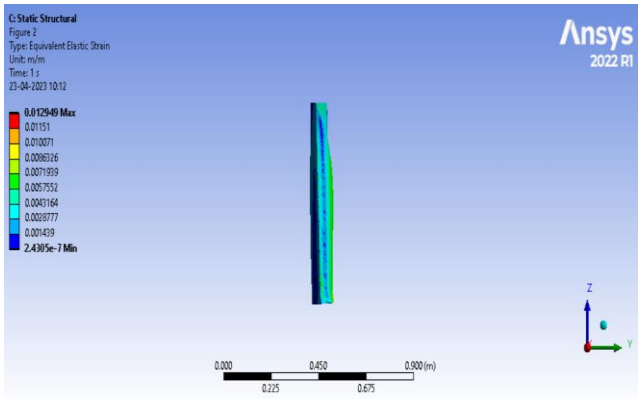

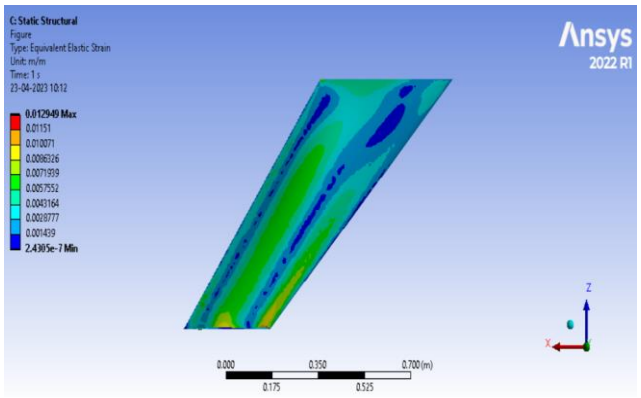

Fig.F.5: Representation of Equivalent elastic strain

The maximum value of Strain is found to be **0.012949** and the minimum value is in the order of e-7 with a precise value of **2.4305e-7**

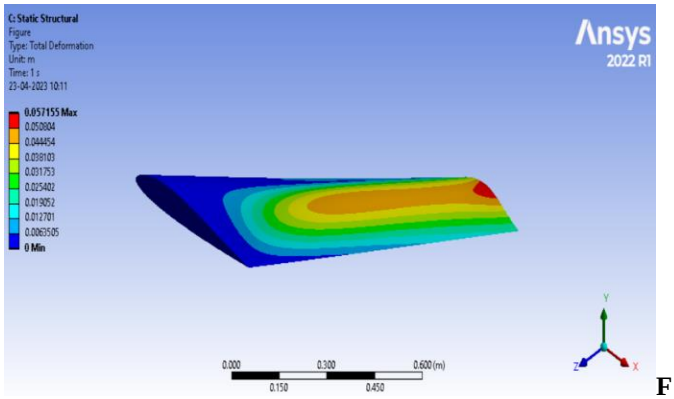

Fig. F.6: Representation of total deformation

The maximum value of Total deformation was found to be **0.057155 m** and is vividly seen in the wing tip as the wing tip acts as the free end of a supposed cantilever beam for instance which is more susceptible to deformation. The minimum value of Total deformation is **0 m** at the fixed part of the wing.

G. Fluent Analysis of wing 2 at an AOA 2°

High precision Fluid flow -Fluent analysis has been performed based on the above-tabulated conditions on the Customised wing 2 with an AOA of 2 degrees and the results are formulated below. Required Solver settings and a detailed method of approach can be accessed by using the accompanying Research datasheet.

Table I: Representation of primary Parameters and Settings used in the analysis

No.	Parameters	Settings
1	Type of Solver	Pressure-Based Solver
2	Energy Equation	On
3	Viscous Model	Two Equations, Standard k - E Turbulent Model
4	Fluid Medium	Air as Ideal Gas
5	Operating Altitude	1500 m
6	Operating Pressure	84643 Pascal
7	Operating Temperature	278.4 K (Correspond to the Altitude).
8	Free Stream Velocity	Mach 2.0.
9	Boundary Condition	a. Inlet as Pressure Far-Field. b. Outlet as Pressure Far-Field.
10	Angle of attack	2 Degrees

Table II: Representation of Mesh size

Cells	Faces	Nodes
1717046	3483859	312346

Table III: Representation of Mesh Quality

Name	Type	Min Orthogonal Quality	Max Aspect Ratio
farfield	TetCell	0.00059586577	466.67949

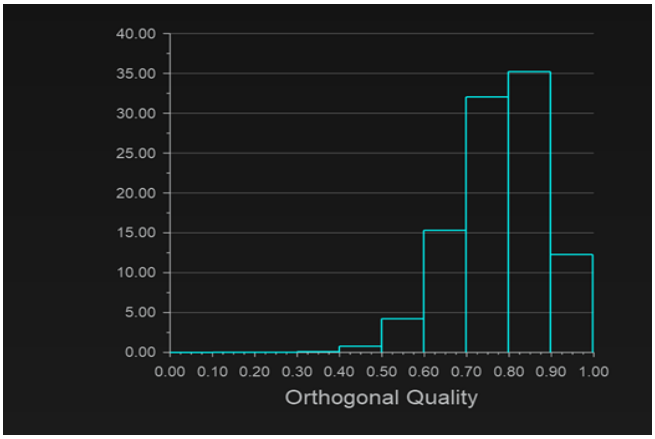

Fig.G.1: Orthogonal Quality chart showing excellent mesh

Table IV: Report definitions (Lift and Drag)

lift	8494.002 N
drag	13741.04 N

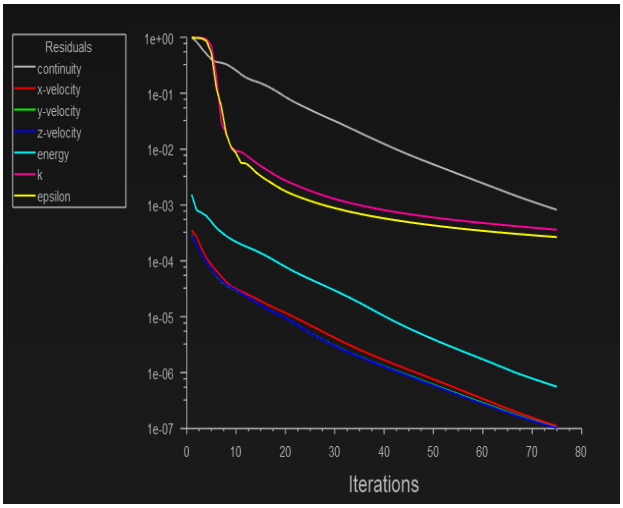

Fig.G.2: Representation of Residual plot

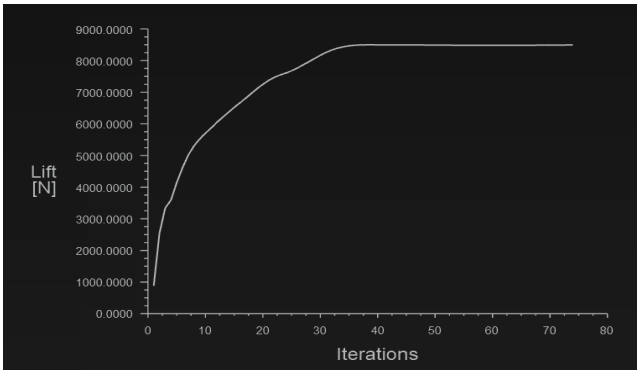

Fig.G.3: Representation of Lift plot

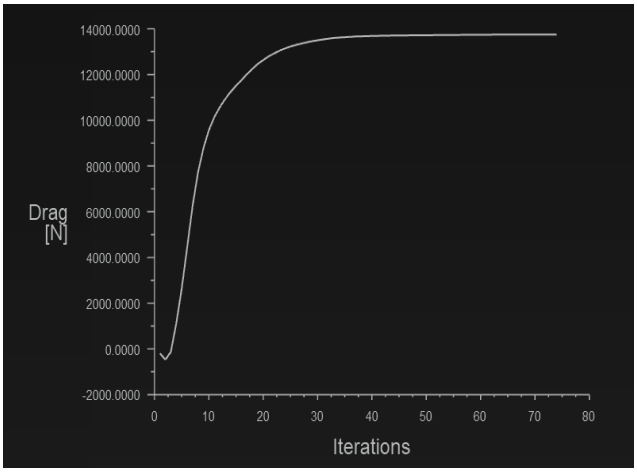

Fig.G.4: Representation of Drag plot

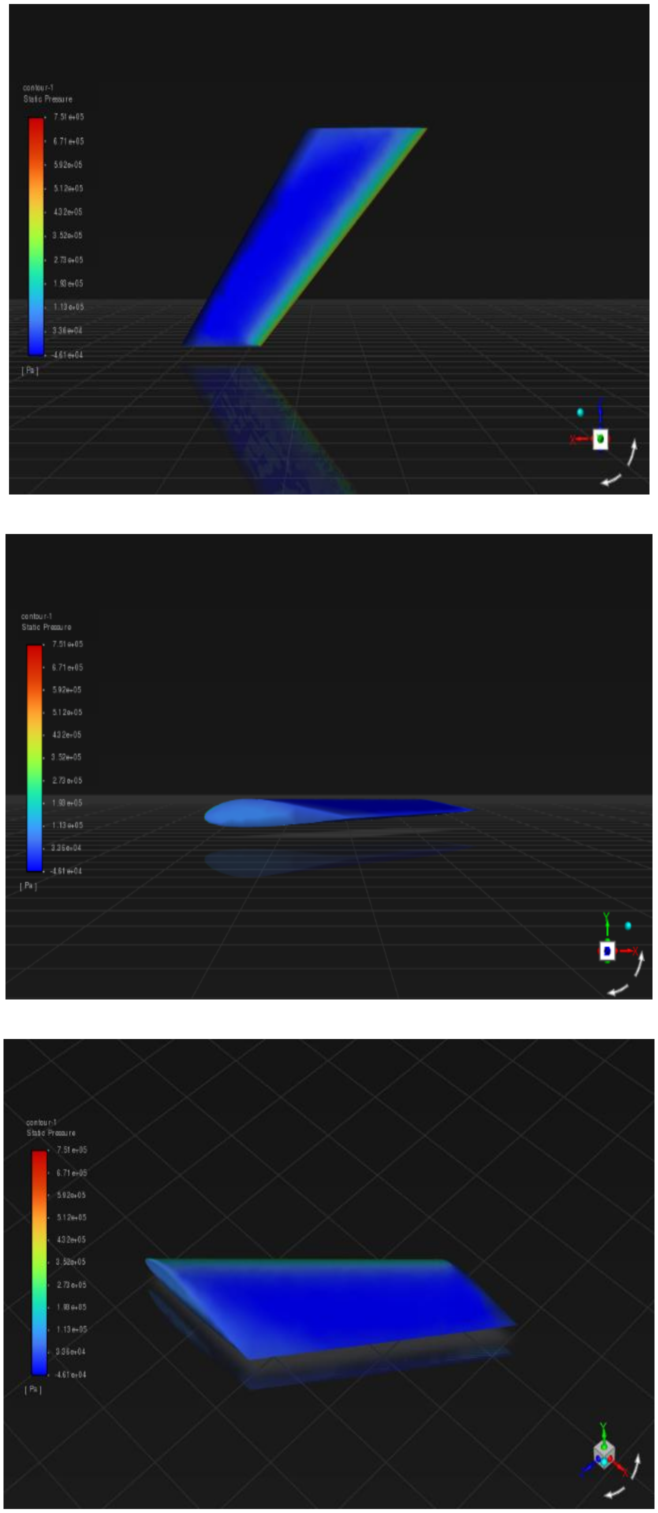

Fig.G.5: Representation of Static pressure contours

The maximum Static pressure value has been found to be 7.51e+05 Pa. The minimum Static pressure value has been found to be -4.61e+04 Pa

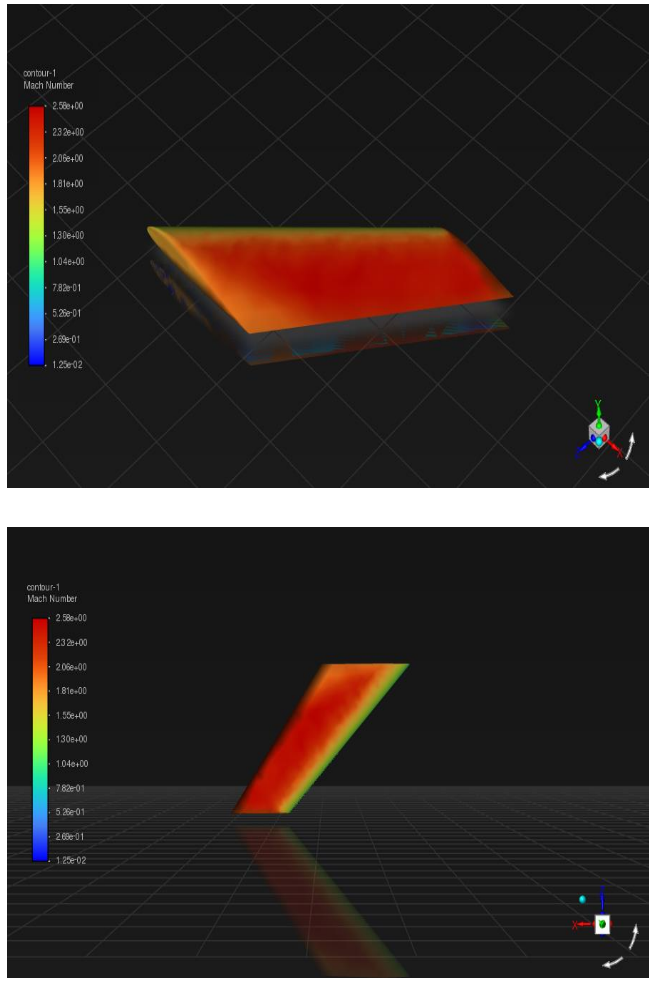

Fig.G.6: Representation of Velocity-Mach contours

The range at which the wing exhibits Mach value lies between 1.8 to 2.58 with 2.58 being the maximum value specifically at the surface of immediate contact with the penetrating air.

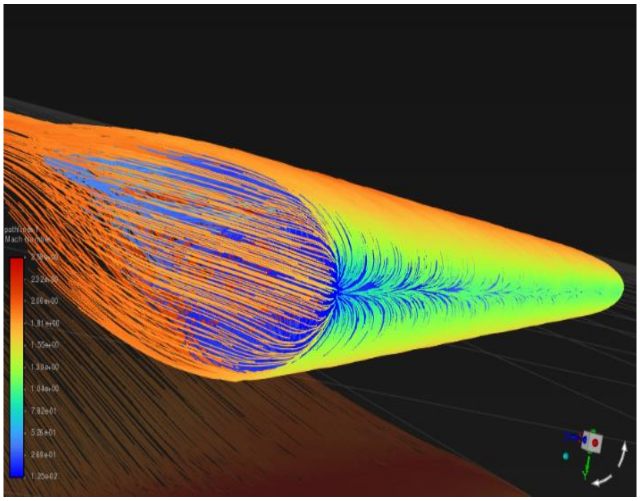

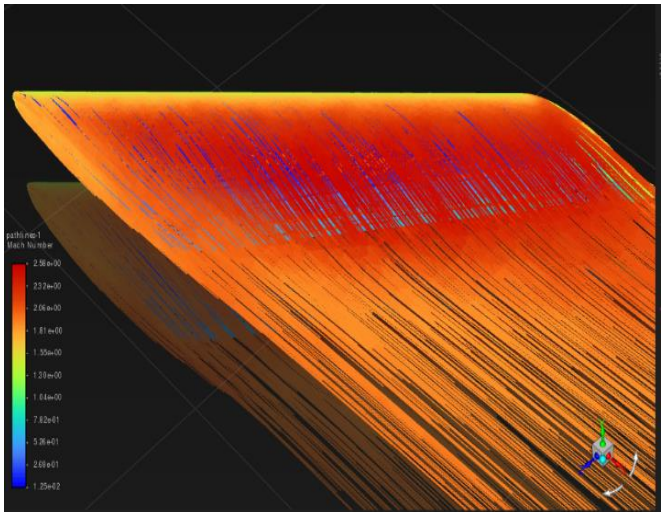

Fig.G.7: Representation of pathlines

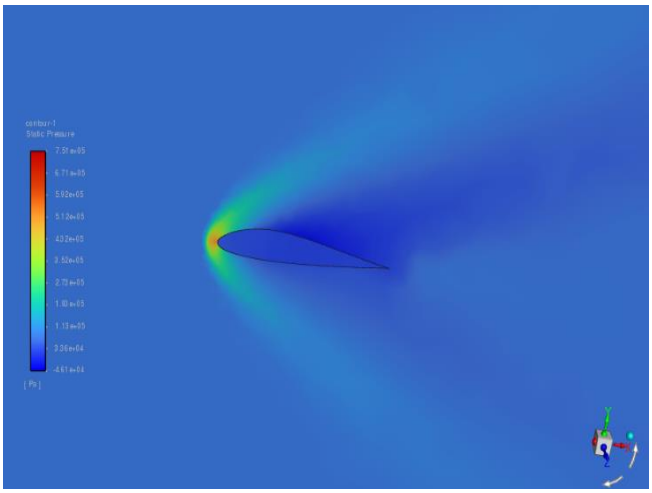

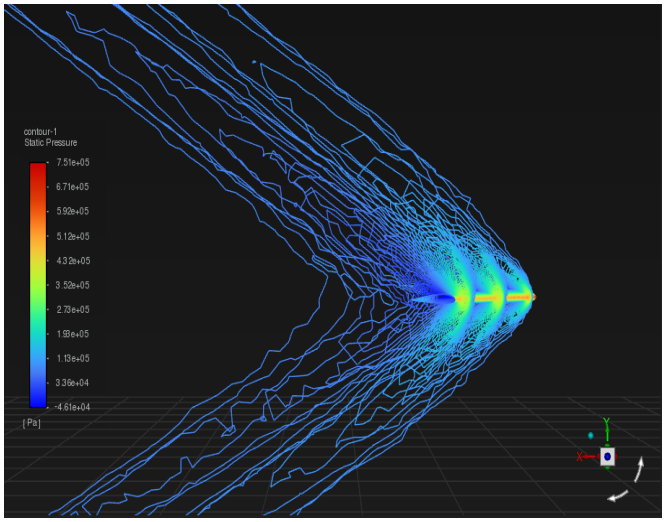

Fig.G.8: Representation of propagation of filled/unfilled shockwaves around the airfoil (Static pressure contour)

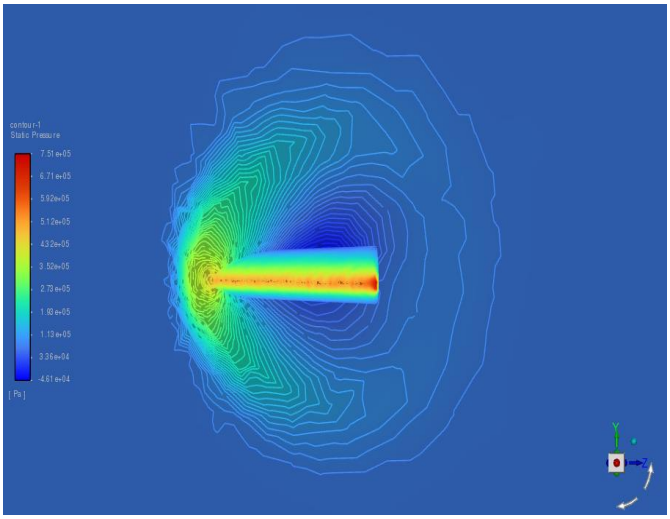

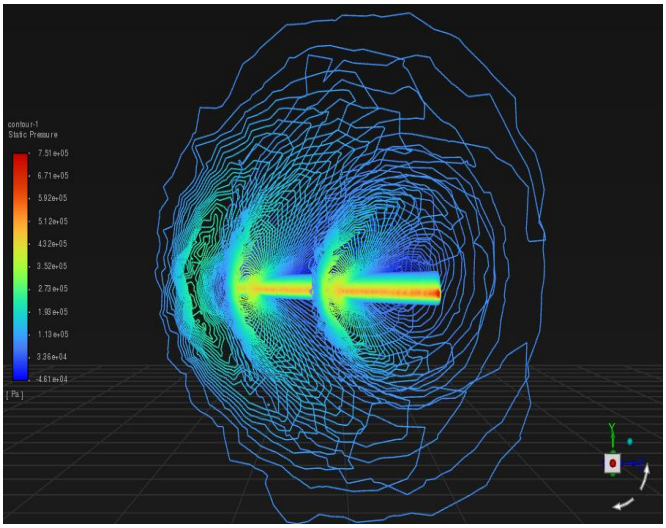

Fig.G.9: Representation of shockwaves on a plane perpendicular to the direction of flow of fluid (Static pressure contour)

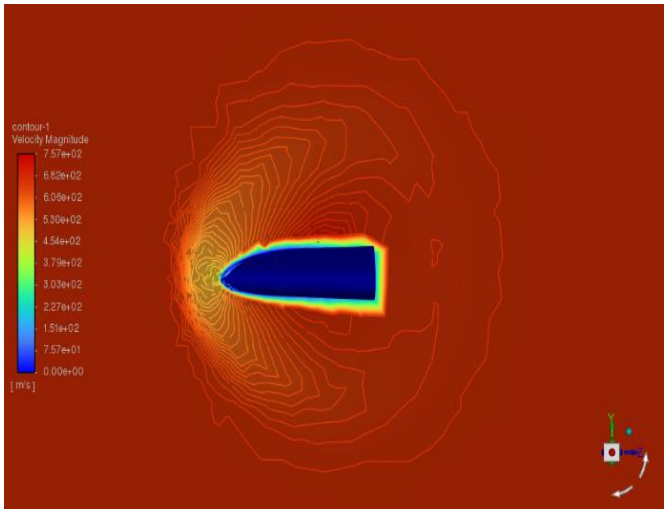

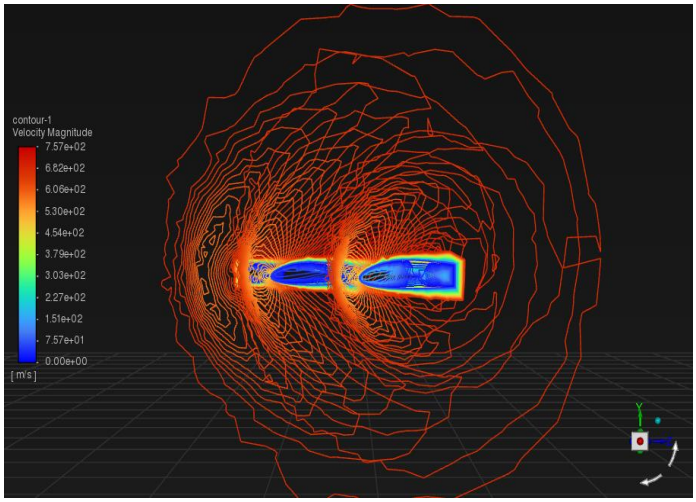

Fig.G.10: Representation of shockwaves on a plane perpendicular to the direction of flow of fluid (Velocity Magnitude contour)

The distribution of velocity magnitude across the wing is clear by the cross-sectional contour view provided by Fig G.10. It shows that the circumferential area of the wing has a maximum velocity of **757 m/s** and the hollow region in the inside is where the minimum velocity of fluid flow is obtained with **0 m/s**

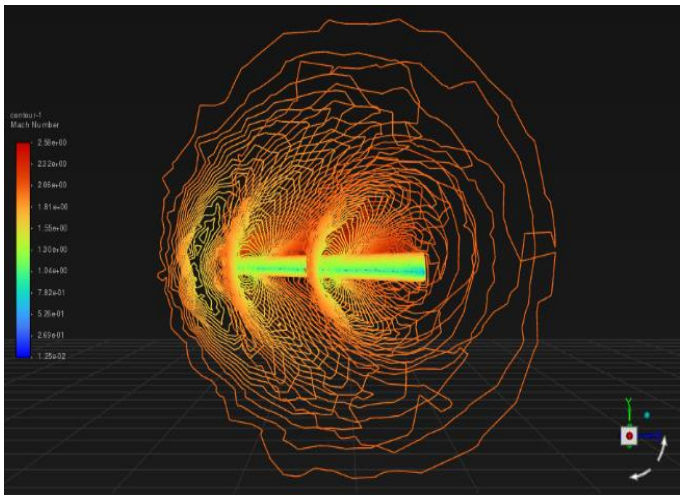

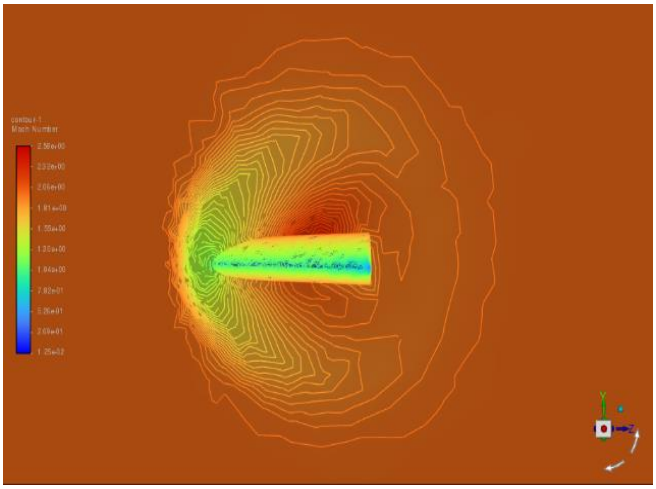

Fig.G.11: Representation of shockwaves on a plane perpendicular to the direction of fluid flow (Velocity-Mach contour)

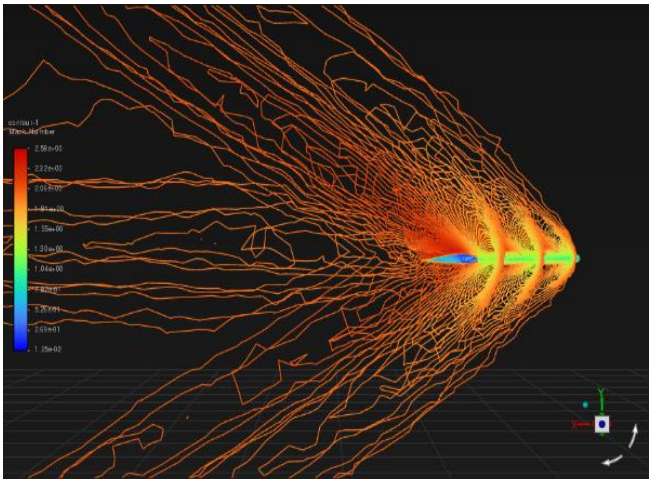

Fig.G.12: Representation of propagation of unfilled shockwaves around the airfoil (Velocity-Mach contour)

H. Structural Analysis of wing 2 at an AOA 2°

units

Unit System	Metric (m, kg, N, s, V, A) Degrees rad/s Celsius
Angle	Degrees
Rotational Velocity	rad/s
Temperature	Celsius

Fig.H.1: Representation of units

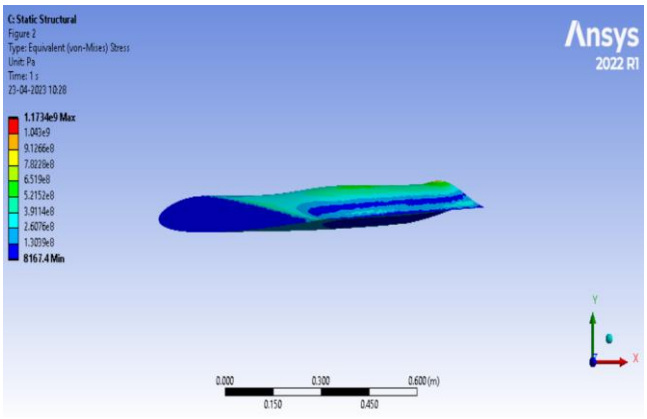

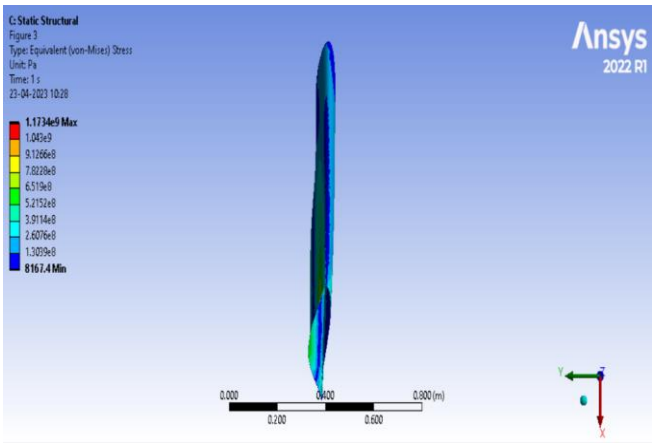

Fig.H.2: Representation of Equivalent stress

The maximum value of Von-mises stress is found to be **1.1734e09 Pa** whereas the minimum value is found to be **8167.4 Pa**

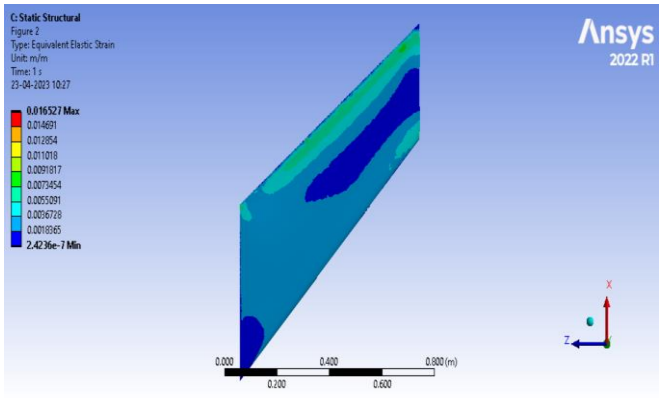

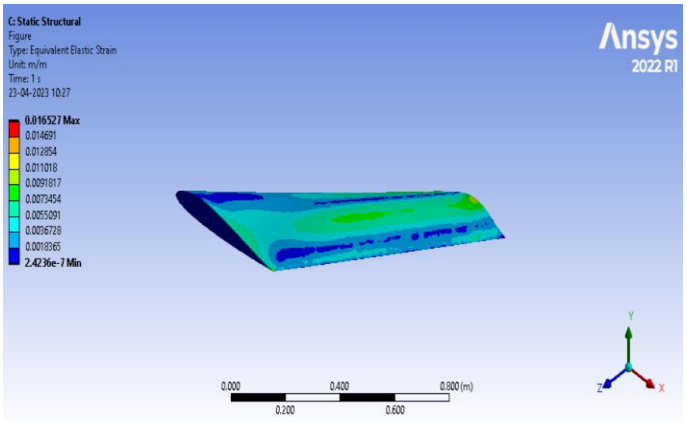

Fig.H.3: Representation of Equivalent elastic strain

The maximum value of Strain is found to be **0.016527** and the minimum value is in the order of e-7 with a precise value of **2.4236e-7**

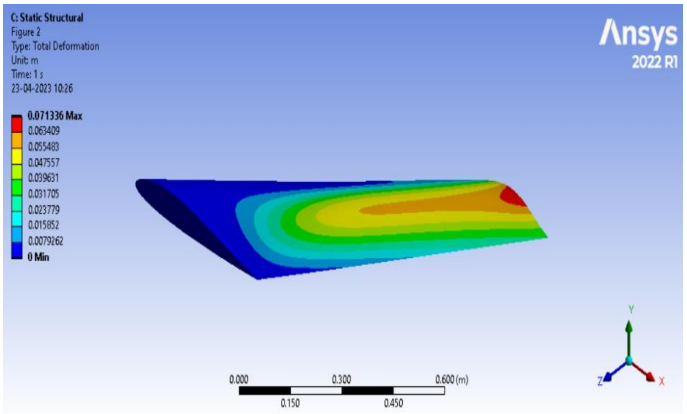

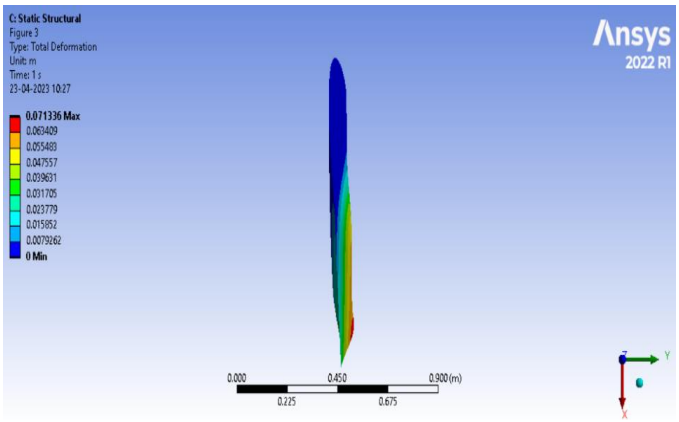

Fig.H.4: Representation of total deformation

The maximum value of Total deformation was found to be **0.071336 m** and is vividly seen in the wing tip as the wing tip acts as the free end of a supposed cantilever beam for instance which is more susceptible to deformation. The minimum value of Total deformation is **0 m** at the fixed part of the wing

I. Comparison of Plots

I.1 AOA VS Total Deformation

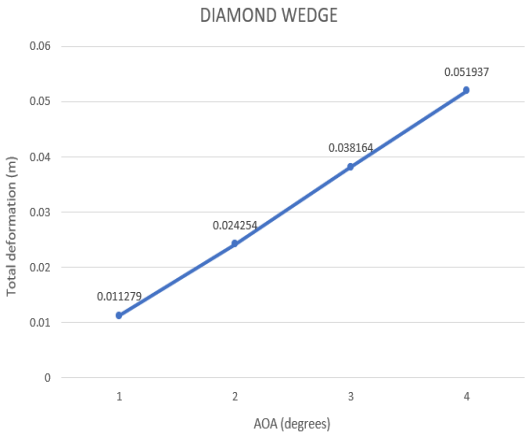

Fig.I.1.1: Plot with AOA on abscissa and Total deformation on the ordinate axis for Diamond wedged wing

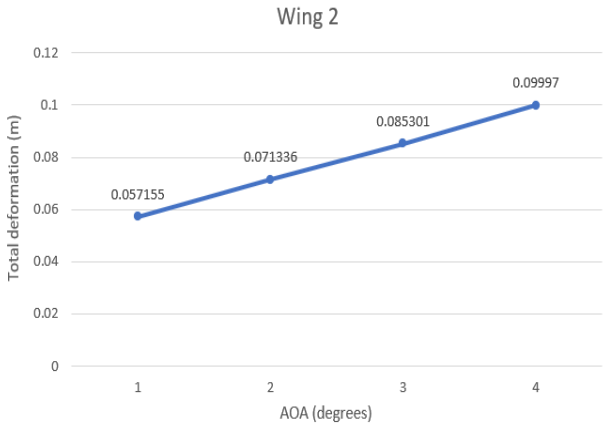

Fig.I.1.2: Plot with AOA on abscissa and Total deformation on the ordinate axis for wing 2

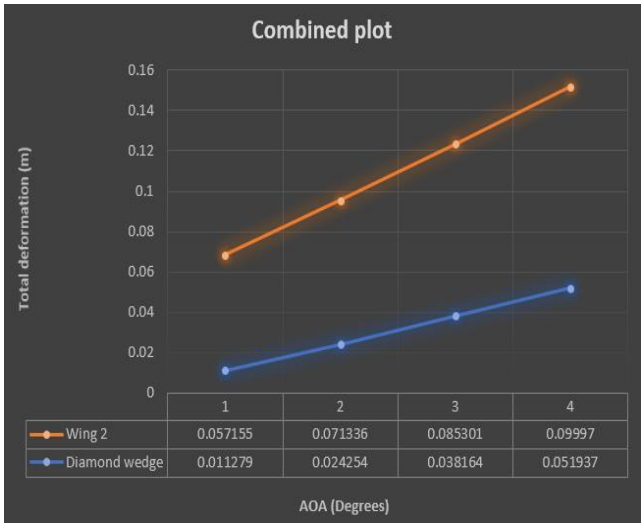

Fig.I.1.3: Combined Plot of both the wings with AOA on the abscissa and Total deformation on the ordinate axis

I.2 AOA VS Stress

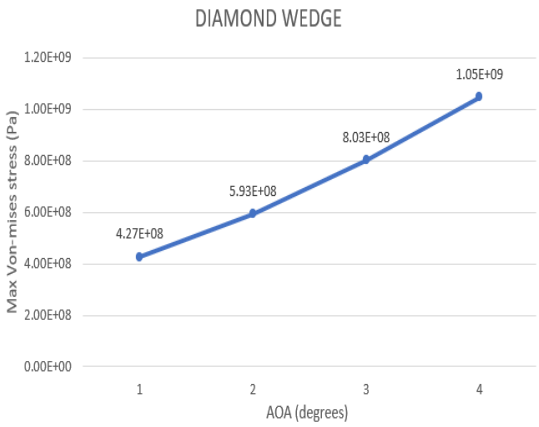

Fig.I.2.1: Plot with AOA on abscissa and Max Von mises stress on the ordinate axis for Diamond wedged wing

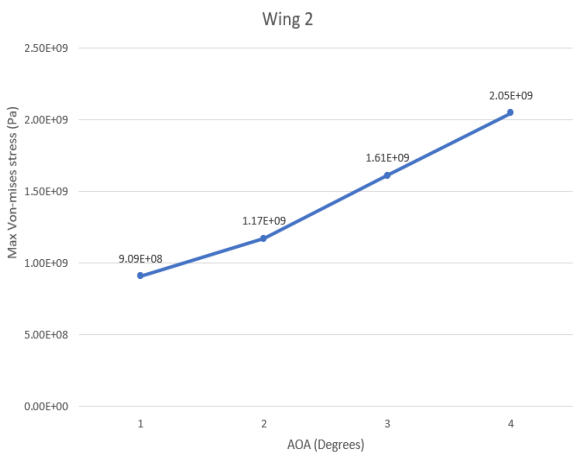

Fig.I.2.2: Plot with AOA on abscissa and Max Von mises stress on the ordinate axis for wing 2

Fig.I.1.3: Combined Plot of both the wings with AOA on abscissa and Von mises stress on the ordinate axis

V. CONCLUSION

The present study has demonstrated that the sheet metal design of an Impractical supersonic wing is susceptible to self-exciting oscillations or flutter effects, not only under Unsteady and Nonlinear aerodynamic conditions but also under Steady and Nonlinear conditions in a similar fashion. Through the use of coupled analysis of fluid flow in Fluent and static structural analysis, the study sheds light on the intricate interplay between aerodynamic forces and structural dynamics, which can lead to complex and potentially catastrophic behaviours. The findings underscore the importance of considering both steady and unsteady aerodynamic conditions in the design and analysis of supersonic wings, as well as the critical role of structural design in mitigating flutter effects. These insights can inform future research and development efforts aimed at enhancing the safety and performance of supersonic aircraft.

VI. ACKNOWLEDGMENT

The authors would like to express their sincere gratitude to Ms. Shivika Lamba for her invaluable assistance in providing an insight on how format a research paper.

REFERENCES

[1] Eric Durand, Time Domain Modelling of Unsteady Aerodynamic Forces on a Flapping Airfoil. Master of Science in Aeronautics and Astronautics, Thesis. (Massachusetts Institute of Technology) 1998. All rights reserved.

[2] Chung-Li Liao and Yee-Win Sunt. Flutter Analysis of Stiffened Laminated Composite Plates and Shells in Supersonic Flow, AIAA JOURNAL Vol. 31, No. 10, October 1993

[3] Chai Y, Gao W, Ankay B, Li F, ZhangC. Aeroelastic analysis and flutter control of wings and panels: A review.International Journal of Mechanical System Dyn. 2021;doi:10.1002/msd2.1201534|CHAIET AL.

[4] Antony Jameson, Luigi Martinelli and John C. Vassberg (2002), Using Computational fluid dynamics for Aerodynamics- A Critical Assessment. Conference: 23rd International Congress of Aeronautical Sciences, Toronto.

[5] Amandeep Singh, Effect of Altitude on missile design, IJSDR. ISSN: 2455-2631. Volume 5 Issue 12

[6] Amit Ramji, Experimental, Numerical and Theoretical Analysis of Supersonic Flow Over A Solid Diamond Wedge. The University of Hertfordshire, 23rd March 2014.

[7] Chen Dongyang, Laith K Abbas, Rui Xiaoting and Wang Guoping, Aerodynamic and static aeroelastic computations of a slender rocket with all-movable canard surface. Journal of Aerospace Engineers, Institution of mechanical engineers. 28th March 2017

[8] John J. Bertin, Aerodynamics for Engineers. Fourth edition, PEARSON

[9] Chao HUANG, Chao YANG, Zhigang Wu and Changhong TANG. Variations of flutter mechanism of a span-morphing wing involving rigid-body motions. January 2018. Chinese Journal of Aeronautics 31(3) doi: 10.1016/j.cja.2017.12.014

[10] Theja Shivaji Tharkude, Dr. Zheng(Jeremy) Li. Simulation Study of Supersonic Natural Laminar Flow on Wing with Biconvex Airfoil. IJERT, ISSN: 2278-0181, Vol-7 Issue 13 March 2018

[11] P. Sturdza, Extensive Supersonic Natural Laminar Flow on the Aerion Business Jet, 45th AIAA Aerospace Sciences Meeting and Exhibit, 8–11 January 2007

[12] Frank A. Woodward (1968). Analysis and Design of Wing-Body Combinations at Subsonic and Supersonic Speeds. Journal of Aircraft, 5(6) ,528-534. doi: 10.2514/3.43979

[13] Karaca HD, O¨ zen GD and Kasnakoglu C. Nonlinear modelling and control of the flow over airfoils using CFD simulations. Simulation Model Practical Theory 2016;67, 29-43.doi: 10.1016/j.simpat.2016.06.009

[14] Roehl, P., Mavris, D., & Schrage, D. (1995). Combined aerodynamic and structural optimization of a high-speed civil transport wing. 36th Structures, Structural Dynamics and Materials Conference. doi:10.2514/6.1995-1222

[15] Richard Fitzpatrick 22nd January 2016, University of Texas Thesis.

[16] Arnold M. Kuethe and Chuen-Yen Chow, Foundations of aerodynamics, Bases of Aerodynamic design, Fifth edition, WILEY

[17] K S, VARUNKUMAR; Nikhil N, Gangamkote (2023), "Fluid-structure interaction methodology to analyse flutter effect on supersonic sheet metal wing design", Mendeley Data, V1, doi: 10.17632/36h7psr4mk